Geochemistry Geophysics Geosystems G3
AN ELECTRONIC JOURNAL OF THE EARTH SCIENCES
Published by AGU and the Geochemical Society

Article
Volume 3, Number 11
21 November 2002
1069, doi:10.1029/2001GC000287
ISSN: 1525-2027

In situ Re-Os analysis of sulfide inclusions in kimberlitic olivine: New constraints on depletion events in the Siberian lithospheric mantle

W. L. Griffin
GEMOC ARC National Key Center, Department of Earth and Planetary Sciences, Macquarie University, NSW 2109, Australia (wgriffin@els.mq.edu.au)

Also at CSIRO Exploration and Mining, North Ryde, NSW 2113, Australia

Z. V. Spetsius
Institute of Diamond Industry, ALROSA Co. Ltd., Mirny, Yakutia 678170, Russia (spetsius@yna.alrosa-mir.ru)

N. J. Pearson and Suzanne Y. O'Reilly
GEMOC ARC National Key Center, Department of Earth and Planetary Sciences, Macquarie University, NSW 2109, Australia (norman.pearson@mq.edu.au; Sue.Oreilly@mq.edu.au)

[1] Os and other highly siderophile elements in mantle-derived peridotites are strongly concentrated into trace amounts of sulfide minerals. We have used a laser-ablation microprobe coupled to a multicollector ICPMS (LAM-MC-ICPMS) to determine the Os isotope composition, Re/Os and Pt/Os of 92 sulfide inclusions in olivine macrocrysts, derived from mantle peridotites, from the Udachnaya kimberlite in the Siberian craton. 26 of these have also been analyzed for Platinum Group Elements and other trace elements by LAM-ICPMS. The sulfides are mixtures of Ni-rich and Fe-rich monosulfide solid solutions (MSS), pentlandite and chalcopyrite, exsolved from MSS bulk compositions. They can be divided into five populations (1, 2, 3A–3C) on the basis of Os content, Os/Pt and Re/Os. The genetic relationships of these groups can be constrained by comparison with published experimental data on element partitioning between MSS and sulfide melts. Group 1 sulfides can be modeled as the MSS residual after low degrees of melting of a primitive mantle source, under sulfur-saturated conditions. Group 2 sulfides are best modeled as mixtures of MSS and alloy phases, formed at low degrees of melting under sulfur-undersaturated conditions; many contain Pt-rich micronuggets. Group 3C sulfides can be modeled as sulfide liquids, or as MSS crystallized from very evolved sulfide liquids. Sulfides of Groups 3A and 3B are interpreted as the products of reaction between MSS of Groups 1 and 2, and liquids of Group 3C. Inclusions of different groups may occur within single olivine grains, suggesting repeated introduction of sulfide melts, followed by annealing and grain growth. Sulfides of Groups 1 and 2, and some 3A sulfides, give Os model ages (T_{MA}) that are geologically reasonable (0–4 Ga). Most Group 3 sulfides contain unsupported ^{187}Os, implying a two-stage history. A negative correlation between T_{MA} and Re/Os is consistent with mixing between residual MSS of Groups 1 and 2, and liquids (3C) derived from a source with a high Re/Os, such as the ca 3.0 Ga eclogites described from Udachnnaya [*Pearson et al.*, 1995c]. Our modeling suggests that sulfides with $^{187}Re/^{188}Os < 0.07$ are unlikely to have been disturbed. Fifty-two grains satisfy this criterion; 45 of these give T_{MA} ages between 2.5 and 3.6 Ga, and 35 are >2.8 Ga. The data suggest that most of the lithospheric mantle beneath the Daldyn kimberlite field formed during the period 3–3.5 Ga, and that lithosphere formation culminated in a major event at ca 2.9 Ga, which may have involved remelting of older eclogites. There is little evidence in the Re-Os data for significant additions to the lithosphere after this time. In situ Re-Os analysis of single sulfide inclusions removes some of the ambiguity involved in the

analysis of whole rock peridotite samples (or even separated olivine grains), where several generations of sulfides may be present. In situ analysis, combined with careful petrographic and chemical study of the sulfide populations, thus can provide more precise temporal constraints on the evolution of lithospheric mantle.

Components: 12,922 words, 11 figures, 5 tables.

Keywords: Lithospheric mantle; Re-Os; sulfides; Siberia; mantle geochemistry.

Index Terms: 1025 Geochemistry: Composition of the mantle; 1035 Geochemistry: Geochronology; 1040 Geochemistry: Isotopic composition/chemistry; 1065 Geochemistry: Trace elements 3670.

Received 2 December 2001; **Revised** 2 July 2002; **Accepted** 30 August 2002; **Published** 21 November 2002.

Griffin, W. L., Z. V. Spetsius, N. J. Pearson, and S. Y. O'Reilly, In situ Re-Os analysis of sulfide inclusions in kimberlitic olivine: New constraints on depletion events in the Siberian lithospheric mantle, *Geochem. Geophys. Geosyst.*, *3*(11), 1069, doi:10.1029/2001GC000287, 2002.

1. Introduction

[2] The continents are underlain by roots of lithospheric mantle, which vary in thickness, composition and thermal state depending on the age and tectonothermal history of the overlying crust [see review by *O'Reilly et al.*, 2001]. To understand the formation and evolution of continents, we need to know the age of the subcontinental lithospheric mantle (SCLM) beneath crustal terrains of different tectonothermal age.

[3] Because Os behaves compatibly in mantle rocks during melting events, whereas Re is less compatible, the Re-Os system provides model ages that can date melt-extraction (''depletion'') events in the mantle, which might in turn reflect the timing of lithosphere stabilization. The Re-Os system in ultramafic rocks also has generally been regarded as relatively resistant to metasomatic disturbance, and hence the most favorable isotopic system for recovering ages of mantle events. Analysis of Os isotope ratios in mantle-derived samples has contributed much of what we currently know about the age of the SCLM. The available cratonic data indicate that at least portions of the SCLM are as old as the overlying Archean crust [*Shirey and Walker*, 1998; *Carlson*, 1999; *Pearson*, 1999]. However, the existing Re-Os dataset for cratonic peridotites also contains many much younger ''ages'', the meaning of which remains unclear. Taken at face value, they could imply that the formation of the SCLM has been essentially continuous throughout geological time.

[4] Recent developments in the in situ analysis of sulfide phases have shown that the Re-Os systematics of mantle-derived peridotites are more complex than earlier supposed. *Alard et al.* [2000] showed by in situ laser-ablation (LAM)-ICPMS analysis that Re and Os in mantle-derived peridotites essentially reside in trace amounts of sulfide phases, confirming the deductions of *Hart and Ravizza* [1996]. More significantly, this in situ analysis allowed the recognition of two general types of PGE patterns in mantle sulfides from spinel peridotite xenoliths. Sulfides enclosed in primary silicate phases were found to have generally higher Os contents and Os/Pt ratios than sulfides occurring in interstitial positions. The former were interpreted as monosulfide solid solutions (MSS) residual after melting, and the latter as trapped sulfide melts, or MSS crystallized from such melts. Most mantle peridotites examined by *Alard et al.* [2000] contain at least two generations of sulfides with very different PGE patterns and Os contents. This diversity suggests that sulfides, and thus Os, are quite mobile within the SCLM.

[5] *Pearson et al.* [2002] have described in detail a technique for the in situ microanalysis of the Re-Os

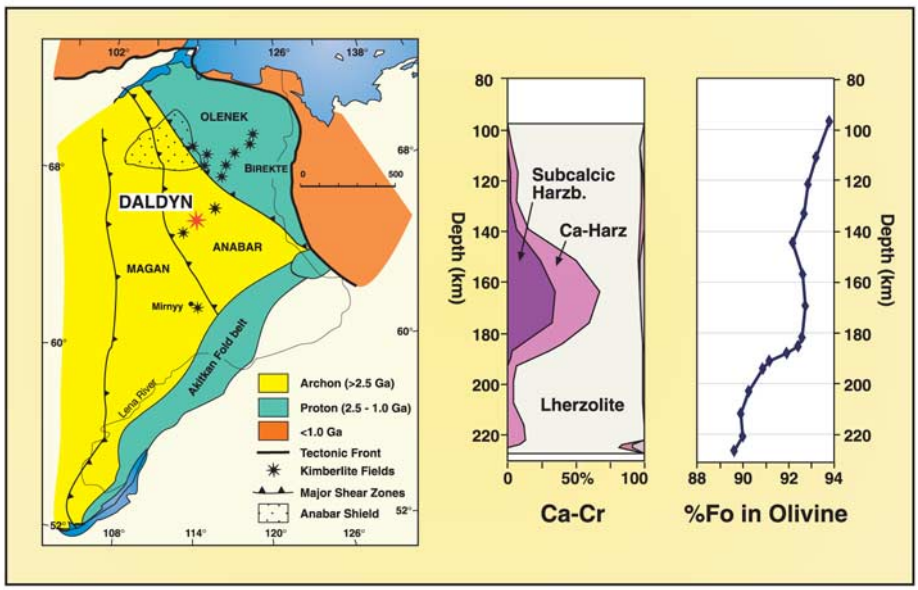

Figure 1. (a) Location map showing the position of the Udachnaya kimberlite (red star), the source of the samples analyzed in this paper, relative to major terranes in the Siberian craton. (b) Distribution of rock types with depth beneath Udachnaya, constructed from data on xenoliths and garnet xenocrysts [after *Griffin et al.*, 1996]. (c) Mean composition of olivine versus depth beneath Udachnaya [after *Gaul et al.*, 2000].

system in sulfides, using a laser ablation microprobe coupled to a multicollector (MC)-ICPMS. They demonstrated that the different types of sulfides described by *Alard et al.* [2002] also can have very different Os-isotope compositions; interstitial sulfides typically have more radiogenic Os. *Alard et al.* [2000] expanded this work, and showed that the interstitial sulfides carry a significant proportion of the Os present in many spinel peridotite xenoliths from alkali basalts.

[6] These results indicate that whole rock Re-Os analyses of mantle-derived peridotites almost inevitably reflect the mixing of different generations of sulfides, and that radiogenic Os has been added to many mantle peridotites at a late stage of their development. This movement of Os may occur independently of Re addition [*Alard et al.*, 2002; *Pearson et al.*, 2002], and the interpretation of the whole rock data in terms of depletion ages therefore becomes ambiguous. However, the development of these new analytical techniques also offers an opportunity to resolve some of the complexity and ambiguity by applying in situ analysis to individual sulfide grains of known petrological and spatial context.

[7] This report presents the results of a reconnaissance study of the age structure of the SCLM beneath one locality in the eastern Siberian Craton, using in situ Re-Os and PGE analysis of sulfides enclosed in mantle-derived olivine grains. This approach allows a relatively rapid survey of the age distribution; a more detailed study involving the serial sectioning of xenoliths and analysis of sulfides relative to microstructural context is in progress.

2. Geological Background, Samples

[8] The samples studied here come from the ca 360 Ma Udachnaya kimberlite pipe, the site of a major diamond mine in the Daldyn kimberlite field within the Archean Daldyn terrane of the Siberian Platform (Figure 1a). The Archean basement is covered by a thick section of Riphean and Paleozoic platform sediments. Sparse zircon U-Pb ages and some Sm-Nd data on the part of the terrane exposed in the Anabar Shield, and on xenoliths from the Udachnaya pipe, suggest crustal formation at ca 3.0 Ga, with minor metamorphic and magmatic events associated with craton amalgamation around 1.9–2.0 Ga [*Rosen et al.*, 1994].

[9] The SCLM beneath the Daldyn field has been described in detail by *Griffin et al.* [1996, 1999]; [see also *Boyd*, 1984; *Boyd et al.*, 1997; *Pokhilenko et al.*, 1999]. It is typical of many Archean SCLM sections in being generally strongly depleted [*Griffin et al.*, 1999], but atypical in showing strong layering (Figure 1b). Harzburgitic rocks, including unusual ''megacrystalline dunites'' (with very coarse olivine enclosing other peridotitic phases) are concentrated between 150–180 km; they are overlain by relatively depleted lherzolites, and underlain by more fertile lherzolites. The mean composition of olivine, as calculated from the compositions of garnet xenocrysts [*Gaul et al.*, 2000] varies between Fo_{92} and Fo_{93} through most of the section, but decreases rapidly to $<Fo_{90}$ between 190 and 210 km depth (Figure 1c).

[10] Olivine grains with sulfide inclusions were selected from coarse (5–8 mm) heavy-mineral concentrate. The large grain size and composition of most grains suggests that they are derived from the megacrystalline peridotites mentioned above, and thus probably are derived from the 150–180 km depth range. The compositions of all grains fall within the range known from xenoliths in this pipe [*Griffin et al.*, 1996; *Boyd et al.*, 1997; *Pokhilenko et al.*, 1999; *Gaul et al.*, 2000] and they therefore are interpreted as fragments of disaggregated peridotites.

[11] Grains were mounted individually in epoxy and polished to reveal sulfide inclusions ranging in diameter from 20 to ca 250 microns. Grains with multiple sulfide inclusions were analyzed and repolished sequentially to reveal deeper inclusions. Some sulfide inclusions, especially smaller ones, were left barely exposed, or just below the surface, to prevent them from popping out of the matrix when ablated, and thus to allow longer ablation times.

[12] Sulfide inclusions were imaged in the electron microprobe; X-ray distribution maps (Figure 2) were used to identify the individual phases and produce modal analyses of individual inclusions. Some sulfide inclusions have negative-crystal forms controlled by the enclosing olivine (Figures 2b, 2e), but most are spherical to oblate (Figures 2a–2d, 2f–2h). Many, especially the larger grains, show radiating expansion cracks lined with films of sulfide, suggesting that some of the sulfide inclusions were molten during ascent to the surface. Nearly all grains that were polished down far enough to reveal a near-median section consist of interfingered Ni-rich and Fe-rich monosulfide solid solutions (MSS; Table 1), surrounded by a discontinuous zone of pentlandite and an outer rim of chalcopyrite (Figures 2a–2d, 2f, 2g). Blocky intergrowths of these phases are also found (Figure 2e), but are much less common. Representative modal analyses and reconstructed bulk compositions (see below) are given in Table 1. No alloy phases were observed in section, but the time-resolved signals collected during the laser-probe analyses demonstrate that many grains contain one or more Pt-rich nuggets up to several microns across. These nuggets commonly occur at or near the surface of grains, but in larger sulfide grains several nuggets may be distributed through the section drilled during the analysis.

3. Analytical Methods

[13] Major-element analyses of the sulfide phases and the host olivines were performed on a CAMEBAX SX50 electron microprobe at GEMOC, Macquarie University, using wavelength dispersive analysis and a range of natural and synthetic standards. The distribution of elements was mapped using a LINK energy-dispersive detector. Modal analyses were obtained by analysis of the x-ray maps using the RockMAS software [*Van Achterbergh*, 2000] (see www.es.mq.edu.au/GEMOC), and combined with electron microprobe analyses of the individual phases to give bulk compositions (Table 1).

[14] The analytical procedures for in situ Re-Os isotopic analysis have been described in detail by *Pearson et al.* [2002] (also see www.es.mq.edu.au/GEMOC). Analyses were carrried out using a Merchantek LUV266 laser microprobe with a modified ablation cell, attached to a Nu Plasma multicollector ICPMS. All ablations were carried out using He as the carrier gas, to enhance sensitivity and reduce elemental fractionation.

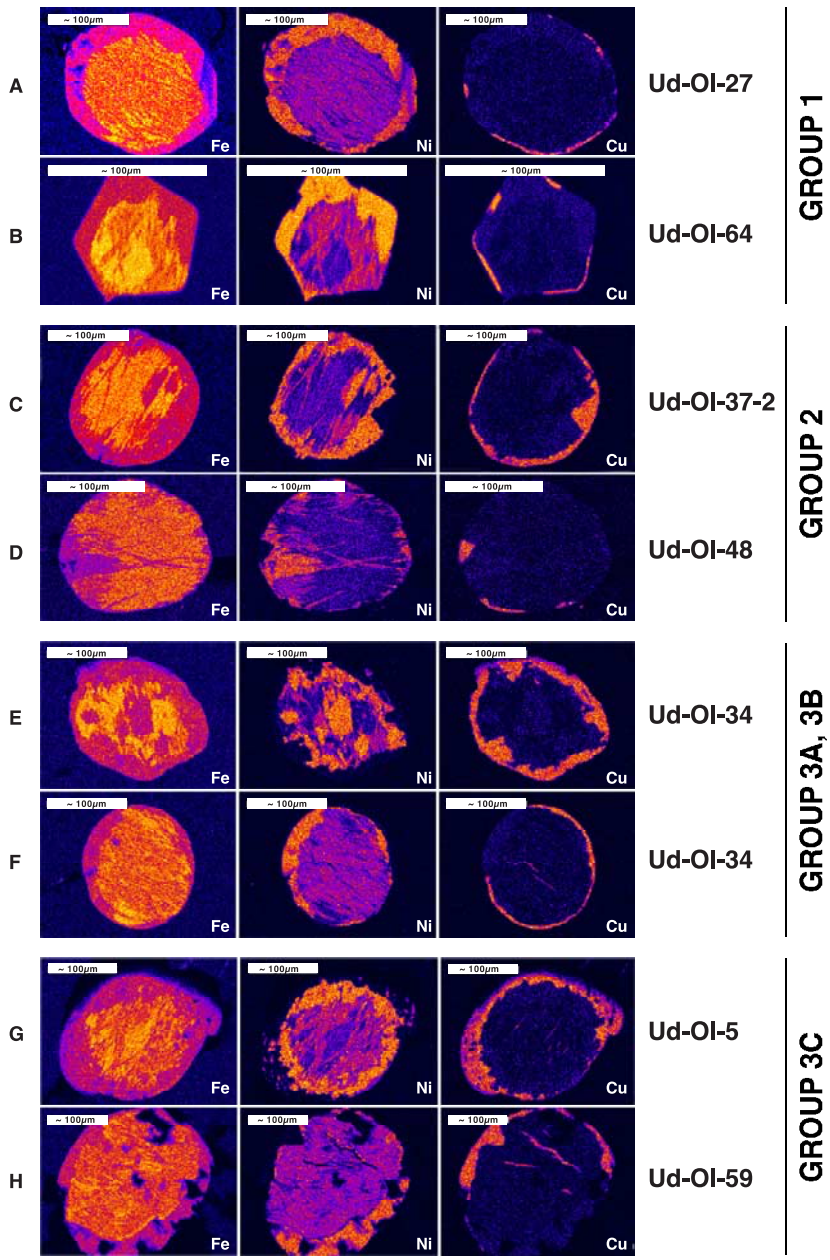

Figure 2. X-ray maps of element distribution in representative sulfide inclusions. (a) Group 1; inclusions 27, 64. (b) Group 2; inclusions 37-2, 48. (c) Groups 3A (inclusion 35) and 3B (inclusion 34). (d) Group 3C; inclusions 5, 59.

Most analyses were carried out at 4 Hz repetition rate and laser energies of 1–2 mJ/pulse, and typical pit diameters were 50–80 microns. A dry aerosol of Ir, produced by a CETAC MCN6000 desolvating nebuliser, was bled into the gas line between the ablation cell and the ICPMS to provide a mass-bias correction with a precision independent of the abundance of Os in the sample. *Pearson et al.* [2002] have demonstrated that, for the Nu Plasma instrument, the relative mass fractionations of Ir, Os and Re are identical within analytical uncertainty, and that the use of Ir for mass bias correction improves precision without introducing a bias on $^{187}Os/^{188}Os$. Table 2 shows that the same results are obtained on both Os standard solutions and laser-ablation analyses using Os and Ir normalization. However, at low Os concentrations, as in the laser-ablation analyses,

Table 1. Modal Analyses, Phase Analyses and Reconstructed Bulk Analyses of Sulfide Inclusions

Modal Analysis (normalized to 100%)

		Pentlandite		Ni-rich MSS		Fe-rich MSS		Chalcopyrite	
	No. Samples	range	mean	range	mean	range	mean	range	mean
Group 1	n = 6	6.9–54.5	27.8	17.9–45.7	29.5	9.5–65.8	37.5	1.3–13.2	5.3
Group 2	n = 8	7.3–38.2	21.5	15.1–41.1	30.1	15.9–69.8	41.4	2.5–16.5	6.9
Group 3A	n = 5	7.1–29.9	25.0	19.3–48.4	33.4	18.0–51.1	35.6	0.4–13.3	5.5
Group 3B	n = 5	6.4–22.0	10.9	18.4–55.7	34.7	37.1–85.1	51.7	0.7–16.7	5.0
Group 3C	n = 10	12.0–30.2	19.9	27.5–49.0	36.2	18.4–50.9	34.5	2.8–23.9	9.5

Mineral Analyses (means)

		Co	Fe	Ni	Cu	Zn	S	O	Sum
Pentlandite	n = 20	0.76	27.2	38.6	0.08	0.03	32.4	0.67	99.8
Chalcopyrite	n = 20	0.00	30.0	0.6	34.2	0.01	34.8	0.47	100.0
Ni-rich MSS									
Grp. 1	n = 7	0.59	39.1	20.6	0.01	0.01	39.3	0.45	99.9
Grp. 2	n = 6	0.54	38.6	20.4	0.03	0.01	39.1	0.61	99.3
Grp. 3A	n = 3	0.56	38.0	21.0	0.04	0.02	39.0	0.68	99.3
Grp. 3B	n = 3	0.44	40.0	19.3	0.03	0.01	38.1	0.54	98.3
Grp. 3C	n = 12	0.50	39.9	19.5	0.02	0.02	38.9	0.74	99.4
Fe-rich MSS									
Grp. 1	n = 6	0.11	51.2	8.5	0.01	0.01	38.4	1.56	99.0
Grp. 2	n = 7	0.12	50.1	9.0	0.05	0.01	38.7	0.79	98.7
Grp. 3A	n = 4	0.08	52.9	6.7	0.06	0.01	39.3	0.47	99.5
Grp. 3B	n = 1	0.04	55.6	3.1	0.02	0.03	38.6	0.27	97.7
Grp. 3C	n = 7	0.16	50.8	9.1	0.01	0.01	38.6	0.37	98.9

Mean Bulk Analyses

		Co	Fe	Ni	Cu	Zn	S	O	Sum
Grp. 1	n = 6	0.46	43.6	16.2	0.66	0.02	38.4	0.39	99.8
Grp. 2	n = 7	0.40	40.6	18.3	1.96	0.01	37.5	0.55	99.3
Grp. 3A	n = 3	0.31	42.6	16.8	2.24	0.02	36.9	0.63	99.5
Grp. 3B	n = 3	0.25	44.1	14.1	2.38	0.01	37.6	0.61	99.0
Grp. 3C	n = 8	0.49	38.5	18.9	3.37	0.03	37.3	0.66	99.3

Atomic Proportions

		Co	Fe	Ni	Cu	S	O
Grp. 1	n = 6	0.005	0.339	0.120	0.005	0.521	0.010
Grp. 2	n = 7	0.004	0.318	0.137	0.014	0.512	0.015
Grp. 3A	n = 3	0.004	0.307	0.140	0.034	0.498	0.017
Grp. 3B	n = 3	0.002	0.365	0.083	0.019	0.514	0.017
Grp. 3C	n = 8	0.005	0.302	0.141	0.023	0.511	0.018

precision is greatly improved by the use of Ir normalization.

[15] Masses 188–194 were measured in Faraday cups, and masses 185 and 187 were measured in ETP ion counters. The ion counters were calibrated initially against the Faraday cups and one another using a two-cycle analysis of a standard Os solution, rather than the sequential analysis of Ir + Os and Re + Ir solutions used by *Pearson et al.* [2002]. During ablation runs, a standard NiS bead with 200 ppm Os and Pt (PGE-A) was analyzed between samples, to monitor and correct any drift in the ion counters. These corrections typically

Table 2. Analyses of Os Standards[a]

Standard		Collector	$^{192}Os/^{188}Os$	1 se	$^{190}Os/^{188}Os$	1 se	$^{189}Os/^{188}Os$	1 se	$^{187}Os/^{188}Os$	1 se	$^{186}Os/^{188}Os$	1 se
JM Bern	Avg n = 22	F+IC	3.07963	0.00022	1.98287	0.00013	1.21932	0.00009	0.10695	0.00004	0.12094	0.00005
	2sd		0.00094		0.00091		0.00037		0.00021		0.00183	
Schoenberg et al. [2000]									0.10694 ± 0.00016			
DTM	avge n = 27	F	3.08141	0.00055	1.98331	0.00012	1.21964	0.00009	0.17376	0.00006	0.12060	0.00004
	2sd		0.00350		0.00119		0.00063		0.00040		0.00079	
DTM (Ir)	avge n = 23	F+IC	3.07543	0.00018	1.98118	0.00010	1.21889	0.00007	0.17375	0.00007	ND	ND
	2sd		0.00184		0.00055		0.00037		0.00049		ND	
Shirey [1997]									0.17429 ± 0.00055			
Lambert et al. [1998]									0.17367 ± 0.00058			
PGE-A	avge n = 40	F+IC	3.07765	0.00146	1.98068	0.00083	1.21856	0.00058	0.10632	0.00008	0.12056	0.00050
	2sd		0.00403		0.00410		0.00180		0.00132		0.00143	
PGE-A (Ir)	avge n = 67	F+IC	3.08033	0.00123	1.98072	0.00061	1.21950	0.00050	0.10638	0.00007	ND	ND
	2sd		0.01348		0.00749		0.00407		0.00048		ND	
I. Horn, J. Chesley (personal communication, 2000)									0.10645 ± 0.00002			

[a] JM Bern Os solution standard, DTM Os standard solution, PGE-A – Os ratios normalized to $^{189}Os/^{192}Os = 0.39593$ [*Volkening et al.*, 1991] and corrected for mass bias using the exponential law. DTM (Ir) standard solution, PGE-A (Ir) – Os ratios normalized to $^{193}Ir/^{191}Ir = 1.6846$ [*Pearson et al.*, 2002] and corrected for mass bias using the exponential law. F+IC – mixed Faraday and ion counter collector setup. ND, not determined; se, standard error.

were less than 1% over a long day's analytical session. The overlap of ^{187}Re on ^{187}Os was corrected by measuring the ^{185}Re peak and using $^{187}Re/^{185}Re = 1.6741$, as described by *Pearson et al.* [2002]. The data were collected using the Nu Plasma time-resolved software, which allows the selection of the most stable intervals of the signal for integration. The selected interval is divided into 40 replicates to provide a measure of the standard deviation and standard error.

[16] The precision and accuracy of the method are discussed in detail by *Pearson et al.* [2002]. Under ideal circumstances (i.e. sulfides $\geq$50 microns in diameter, and containing at least 40 ppm Os), an internal precision for $^{187}Os/^{188}Os$ of 0.1–0.3% (2SE) is routinely obtained (Table 2); for smaller grains or lower Os contents (<5–10 ppm), an internal precision of 1–2% is routine. The external reproducibility of $^{187}Os/^{188}Os$ for the PGE-A standard over several months is ±0.00048 (2sd; Table 2), and the mean value of $^{187}Os/^{188}Os$ is indistinguishable from that derived by TIMS analysis. Repeated analysis of 25 ppb standard Os solutions using the same collector configuration gives a similar or better external reproducibility (Table 2). The Re-Os data for the sulfides are reported in Table 3.

[17] During this work Os and Pt contents were estimated by comparing the signal intensity on the sample to that obtained on the PGE-A standard. The accuracy of these data is limited by variations in ablation conditions, the lack of an internal standard, the known small compositional heterogeneity of the particular bead of PGE-A used as the isotopic standard, and the probability that maximum signals are not achieved during short runs on small grains. There also is a nugget effect in the distribution of Pt within some sulfide inclusions (seen in the time-resolved analysis). Despite the uncertainties in absolute Os contents, the Os/Pt ratios reported here (Table 3) are believed to be representative of the volume sampled; Re/Os ratios are expected to be accurate within 10% [*Pearson et al.*, 2002].

[18] Some individual sulfides that were not obliterated during the Re-Os analysis were repolished and analyzed for trace elements using a laser

Table 3. (Representative Sample). [Re-Os Analyses of Sulfide Inclusions] [The full Table 3 is available in the HTML version of the article at http://www.g-cubed.org.]

Sample[a]	$^{187}Os/^{188}Os$	±2se	$^{187}Re/^{188}Os$	±2se	Os ppm	Pt ppm	Os/Pt	Re/Os	Os_I[b]	T_{RD}[b]	T_{MA}	2sd[c]	%Fo, Ol	Group
Ud-Ol-1	0.10573	0.00020	0.00638	0.00015	650	115	5.7	0.0014	0.10569	3.10	3.14	0.03	91.5	2
Ud-Ol-2	0.10696	0.00017	0.02390	0.00092	150	10	15	0.0051	0.10682	2.94	3.10	0.03	92.4	1
Ud-Ol-3	0.10487	0.00054	0.00076	0.00010	550	110	5.0	0.0002	0.10487	3.22	3.22	0.08	93.3	2
Ud-Ol-4	0.10559	0.00094	0.00553	0.00012	240	15	16	0.0012	0.10556	3.12	3.16	0.14	92.5	1
Ud-Ol-5	0.12004	0.00134	0.13828	0.00168	15	15	1.0	0.0294	0.11921	1.15	1.56	0.31	93.2	3C
Ud-Ol-6	0.10768	0.00144	0.01092	0.00096	400	145	2.8	0.0023	0.10761	2.83	2.90	0.22	92.6	2
Ud-Ol-7	0.10862	0.00200	0.03333	0.00054	30	5	6.0	0.0071	0.10842	2.71	2.92	0.31	92.0	3B
Ud-Ol-8	0.14474	0.00580	0.26502	0.01040	10	0.5	20	0.0563	0.14314	−2.46	−8.33		91.9	3B
Ud-Ol-9	0.10955	0.00024	0.01845	0.00034	60	30	2.0	0.0039	0.10943	2.57	2.67	0.04	92.6	3A
Ud-Ol-9-2	0.10614	0.00014	0.00452	0.00003	67	0.3	256	0.0010	0.10611	3.04	3.07	0.02	92.6	1
Ud-Ol-10	0.63784	0.01860	3.45410	0.12400	5	50	0.1	0.7340	0.61706	−100	9.00		92.5	3C
Ud-Ol-11	0.88191	0.19200	17.48010	3.20000	2	3	0.5	3.7145	0.77676	−100	2.60	0.95	91.6	3C
Ud-Ol-11-3	0.28781	0.00360	1.71835	0.00980	19	237	0.1	0.3651	0.27748	−28.2	6.92		91.6	3C
Ud-Ol-13	0.22968	0.00560	1.08125	0.02600	5	5	1.0	0.2298	0.22318	−16.4	8.50		91.6	3C
Ud-Ol-14	0.10560	0.00013	0.00282	0.00004	151	5	28	0.0006	0.10558	3.12	3.14	0.02	91.8	1
Ud-Ol-16	0.12022	0.00124	0.04319	0.00380	50	70	0.7	0.0092	0.11996	1.04	1.12	0.22	92.1	3A
Ud-Ol-17	0.11010	0.00120	0.05339	0.00074	350	220	1.6	0.0113	0.10978	2.52	2.84	0.20	93.0	2
Ud-Ol-18	0.16688	0.00900	0.58921	0.02200	15	95	0.2	0.1252	0.16334	−5.69	11.60		93.5	3C
Ud-Ol-19	0.10663	0.00050	0.03440	0.00200	56	6	9.0	0.0073	0.10642	3.00	3.24	0.09	93.0	3B
Ud-Ol-20	0.10554	0.00110	0.00738	0.00026	2600	325	8.0	0.0016	0.10550	3.13	3.18	0.16	91.7	2
Ud-Ol-21	0.11254	0.00840	0.04057	0.00260	3	0.3	10	0.0086	0.11229	2.16	2.36	1.35	92.9	3B
Ud-Ol-22	0.11464	0.00044	0.09657	0.00064	85	15	5.7	0.0205	0.11406	1.90	2.38	0.08	92.8	3B
Ud-Ol-23A	0.10894	0.00015	0.05163	0.00018	111	7	15	0.0110	0.10863	2.68	3.02	0.02	89.2	1
Ud-Ol-23B	0.11252	0.00158	0.05085	0.00122	20	4	5.0	0.0108	0.11221	2.17	2.43	0.27	89.2	3B
Ud-Ol-24	0.11179	0.00040	0.05973	0.00300	530	140	3.8	0.0127	0.11143	2.28	2.61	0.09	90.3	2
Ud-Ol-26	0.11147	0.00190	0.02150	0.00164	10	0.5	20	0.0046	0.11134	2.29	2.40	0.30	91.5	3B
Ud-Ol-26-2	0.11034	0.00108	0.00764	0.00015	19	1	25	0.0016	0.11029	2.44	2.49	0.16	91.5	3B
Ud-Ol-27	0.10754	0.00020	0.01415	0.00048	330	20	17	0.0030	0.10745	2.85	2.94	0.03	92.6	1
Ud-Ol-28	0.11596	0.00200	0.07975	0.00140	135	150	0.9	0.0169	0.11548	1.70	2.02	0.36	92.8	3A
Ud-Ol-29	0.12779	0.00340	0.21020	0.02400	5	1.5	3.3	0.0447	0.12652	0.07	−0.25		92.5	3C
Ud-Ol-30	0.11366	0.00122	0.00160	0.00007	2750	2000	1.4	0.0003	0.11365	1.96	1.97	0.18	91.4	2
Ud-Ol-31	0.11005	0.00030	0.03121	0.00030	2800	575	4.9	0.0066	0.10986	2.51	2.68	0.05	92.6	2
Ud-Ol-32	0.13482	0.00136	0.24655	0.00860	10	35	0.3	0.0524	0.13334	−0.96	−3.10		92.6	3C
Ud-Ol-32-2	0.11194	0.00026	0.05757	0.00144	81	58	1.4	0.0122	0.11159	2.26	2.57	0.05	92.6	3A
Ud-Ol-33	0.10506	0.00320	0.00251	0.00020	130	5	26	0.0005	0.10505	3.19	3.21	0.43	91.0	1
Ud-Ol-34	0.13101	0.00460	0.22172	0.01320	40	5	8.0	0.0471	0.12968	−0.40	−1.35		93.9	3B
Ud-Ol-35	0.11504	0.00024	0.10994	0.00152	150	40	3.8	0.0234	0.11437	1.86	2.41	0.06	93.0	3A
Ud-Ol-35-2	0.12787	0.00034	0.19798	0.00640	100	110	0.9	0.0421	0.12668	0.05	−0.26		93.0	3A
Ud-Ol-36	0.10414	0.00116	0.01583	0.00028	2100	365	5.8	0.0034	0.10405	3.33	3.45	0.17	93.3	2
Ud-Ol-36-2A	0.10739	0.00010	0.00809	0.00007	600	5	120	0.0017	0.10734	2.87	2.92	0.02	93.3	1
Ud-Ol-36-2B	0.10673	0.00026	0.00757	0.00082	212	7	29	0.0016	0.10668	2.96	3.01	0.04	93.3	1
Ud-Ol-37-2	0.10871	0.00052	0.03481	0.00050	450	105	4.3	0.0074	0.10850	2.70	2.92	0.08	92.6	2
Ud-Ol-38-2	0.15650	0.00182	0.58785	0.02600	50	40	1.3	0.1249	0.15296	−4.35	8.84		92.6	3A
Ud-Ol-39	0.15439	0.00540	0.56046	0.04600	6	6	1.0	0.1191	0.15101	−3.70	9.56		92.2	3C
Ud-Ol-40	0.10531	0.00064	0.01570	0.00320	440	265	1.7	0.0033	0.10522	3.17	3.28	0.12	91.4	2
Ud-Ol-41	0.11419	0.00042	0.05402	0.00120	324	476	0.7	0.0115	0.11386	1.93	2.17	0.08	92.3	2
Ud-Ol-43	0.14130	0.00700	0.36923	0.01880	15	20	0.8	0.0785	0.13908	−1.83	−34.6		93.0	3C
Ud-Ol-43-2	0.13009	0.00190	0.30889	0.00270	11	3	3.7	0.0656	0.12823	−0.18	−2.03		93.0	3C
Ud-Ol-44	0.11781	0.00540	0.01948	0.00220	5	0.5	10	0.0041	0.11770	1.37	1.43	0.84	93.2	3B
Ud-Ol-46	0.12039	0.00048	0.13813	0.00520	525	250	2.1	0.0294	0.11956	1.10	1.49	0.16	91.1	2
Ud-Ol-47	0.11615	0.00036	0.08074	0.00102	125	50	2.5	0.0172	0.11566	1.67	2.00	0.07	90.9	3A
Ud-Ol-48	0.10724	0.00026	0.00382	0.00042	20,000	6000	3.3	0.0008	0.10722	2.88	2.91	0.03	92.9	2
Ud-Ol-49	0.11363	0.00026	0.09887	0.00380	150	130	1.2	0.0210	0.11304	2.05	2.59	0.08	92.7	3A

[a] Analyses labeled −2, −3 etc represent different sulfide inclusions in a single olivine grain; analyses labeled A, B etc. represent replicate analyses of the same sulfide inclusion.

[b] Calculated at 360 Ma, using measured $^{187}Re/^{188}Os$ and decay constant of 1.666E-11.

[c] Propogated 2SE analytical uncertainties on $^{187}Os/^{188}Os$ and $^{187}Re/^{188}Os$. CHUR has $^{187}Os/^{188}Os = 0.127$ and $^{187}Re/^{188}Os = 0.40186$. Analyses labeled AOUd-; data from *Alard et al.* [2000] and *Pearson et al.* [2002].

microprobe attached to an Agilent 7500 ICPMS and methods described by *Alard et al.* [2000]. External standards were a homogeneous sample of PGE-A, and the NIST610 glass standard. Data were reduced using the in-house GLITTER software (see www.es.mq.edu.au/GEMOC/). Sulfur was used as the internal standard for a first data reduction against PGE-A, to give data for the PGE, Cu, Au, As and Se. The Cu value derived from this reduction was then used as the internal standard for a second data reduction against NIST610, giving data for Co, Zn, Mo, Ag, Cd, In, Sn, Sb, Re, Te, W, Pb and Bi. Because of the large differences between the matrices, the elemental concentrations derived from the NIST610 glass are regarded as semiquantitative. Representative analyses are given in Table 4.

4. Results

4.1. Elemental Data

[19] The results of the LAM-MC-ICPMS analyses are given in Table 3, together with the composition of the host olivine grains. The analyzed sulfides show a wide range in Os contents, Os/Pt and Re/Os. Plots of Os/Pt and Re/Os versus Os content (Figure 3) allow the division of the sulfides into five populations. *Group 1* has high Os contents (67–600 ppm, median 180 ppm), high Os/Pt (9–256) and low Re/Os (median 0.004). *Group 2* has higher Os overall contents (320 ppm-2%; median 650 ppm), low Os/Pt (<1–8, median 3.3) and low Re/Os (median 0.0033). *Group 3A* sulfides have lower Os contents (40–225 ppm, median 119 ppm) and low Os/Pt (<1–7, median 2.0), but generally higher Re/Os; *Group 3B* sulfides have still lower Os contents (3–85 ppm, median 20 ppm) but higher Os/Pt (median 8.3), while showing a bimodal distribution of Re/Os; *Group 3C* sulfides have very low Os contents (median 5 ppm), low Os/Pt (median 1.0) and high Re/Os. The Group 3 sulfides have generally higher Re/Os than the Group 1 and Group 2 sulfides, and the mean Re/Os increases as mean Os content decreases from Group 3A (0.014) to Group 3C (0.185). Of the 92 grains successfully analyzed, Groups 1 and 3A each make up 16% of the total, Group 2 = 26%, Group 3B = 13%, and Group 3C = 28%.

[20] Modal analyses and reconstructed bulk compositions were calculated only for inclusions that had been polished down approximately halfway. Despite this precaution, the results show wide ranges in composition; some of the scatter no doubt reflects sectioning effects, and in particular the irregular distribution of chalcopyrite and pentlandite (Figure 2). However, some of the differences in the mean bulk composition of sulfides from the different groups (Table 1) probably are significant. Group 1 sulfides have lower Ni and Cu than Group 2 sulfides, Group 3 sulfides have higher mean contents of Cu than those of Groups 1 and 2, and Cu and Ni are highest, and Fe lowest, in Group 3C. Group 3A sulfides have the lowest S contents. All have MSS bulk compositions, with S = 51 ± 1.5 at %. The mean S content of Group 2 sulfides probably is a maximum value, since the Pt-rich micronuggets, inferred to be alloy phases, are not included in the modal analysis.

[21] There is little correlation between these groups and the composition of the host olivine (Table 3), which is not surprising since several types of sulfide may occur as inclusions in a single olivine grain (see below). However, most sulfides in the least magnesian olivines ($\leq Fo_{92}$) are from Groups 1 and 2, and the host olivines of these groups have the lowest mean %Fo (92.1–92.2). Group 3B sulfides all occur in olivines with Fo $\geq$92.9%, but this may be coincidental.

[22] LAM-ICPMS trace element data on the sulfides (Table 4) show a broad correlation with the Os contents and Os/Pt ratios derived from the LAM-MC-ICPMS analysis, especially for those sulfides where Pt is not obviously distributed in nuggets, and confirm the differences among the sulfide populations defined above. The replicate analyses of three sulfide grains (S53, S54, S67-2) show significant local variations in the contents of the PGE and in Re/Os, which makes direct comparison with the MC-ICPMS data difficult. In many cases, the PGE analyses were carried out on small rem-

Table 4. (Representative Sample). [Trace Element Analyses of Sulfide Inclusions] [The full Table 4 is available in the HTML version of the article at http://www.g-cubed.org.]

Sample	S23	S27 (1)	S58	S64-3	S67-2A	S67-2B	S67-6	mean
Group	1	1	1 Pn,Cpy	1	1	1	1	**Grp 1**
% Ni	11.1	13.7	37.2	24.5	8.2	19.1	27.2	**20**
% Cu	2.27	0.09	3.68	0.13	0.52	2.7	2.95	**2**
Co	1019	717	4732	2673	1166	1991	2948	**2178**
Zn	120	7	1387	12	26	14	16	**226**
As	2.32	1.63	65.5	0.41	6.53	20.7	18.8	**17**
Se	128	79	176	130	184	218	270	**169**
Mo	5.04	6.68	19.58	4.17	47.4	42.4	53.7	**26**
Ru	154	194	641	222	52.9	81	138	**212**
Rh	23.1	37.6	41.5	33.4	11.4	18.0	26.1	**27**
Ag	14.3	0.496	2901	0.516	4.02	10.29	8.46	**420**
Pd	6.42	0.430	27.1	2.08	1.23	5.1	14.8	**8**
Cd	1.41	0.087	10.0	0.471	0.118	1.14	<0.057	**2**
In	0.060	0.011	0.5	<0.0016	0.120	0.317	<0.0017	**0.2**
Sn	9.08	1.41	122	0.225	21.9	3.19	0.077	**23**
Sb	0.106	0.04	2.78	0.043	0.43	0.452	0.349	**1**
Te	16.9	19.4	19.0	25.0	37.7	29.9	44.8	**28**
W	0.381	0.41	38.4	0.031	0.10	0.199	<0.035	**7**
Re	0.219	0.094	0.42	0.288	0.590	0.592	0.837	**0.4**
Os	87.6	160	238	249	62.4	85.7	157	**149**
Ir	47.3	85.5	135	116	30.2	60.0	92.2	**81**
Pt	6.69	5.08	16.1	1.02	17.0	17.2	19.1	**12**
Au	0.254	0.24	640	0.095	27.3	0.106	0.102	**95**
Pb	9.38	3.41	90.9	1.89	13.8	12.4	14.0	**21**
Bi	0.804	0.412	10.1	1.91	1.95	1.36	1.12	**3**
Re/Os	0.0025	0.0006	0.0018	0.0012	0.0095	0.0069	0.0053	**0.0040**
Os/Pt	13.1	31.5	14.8	244	3.7	5.0	8.2	**46**

Sample	S50	S46	S64-5	S53-3	mean	S9	S32-2	S47	S66-5	S67-5	mean	S57
Group	2	2	2	2 Pn, Cpy	**Grp 2**	3A Pn, Cpy	3A Pn, Cpy	3A Pn, Cpy	3A Cpy	3A	**Grp 3A**	**3B**
% Ni	26.1	14.0	20.9	37.2	**25**	29.1	29.7	28.8	11.3	25.8	**25**	17.5
% Cu	0.66	0.58	0.42	1.80	**1**	0.97	2.77	3.58	5.7	1.43	**3**	1.09
Co	1223	934	2813	7263	**3058**	3043	2814	4433	1241	3298	**2966**	1684
Zn	644	20	7	3977	**1162**	6.46	146	2840	908	1472	**1075**	29
As	73.7	<0.58	8.49	<21.4	**41**	1.73	2.47	50.8	8.61	34.3	**20**	4.31
Se	1710	383	176	511	**695**	10.3	154	416	96	281	**192**	234
Mo	28.0	13.2	8.0	12.7	**15**	13.9	1.89	18.3	19.7	21.9	**15**	13.5
Ru	1013	229	65.0	2180	**872**	109	115	647	202	63.4	**227**	77.8
Rh	186	13.3	13.3	220	**108**	17.1	18.0	73.3	24.8	12.3	**29**	15.1
Ag	109	49.2	0.933	24.1	**46**	1.68	3.24	1156	6.02	5.85	**235**	136
Pd	<7.61	34.3	5.72	18.5	**19**	0.099	102.34	67.3	222	39.5	**86**	19.6
Cd	<4.59	0.278	<0.058	88.4	**44**	0.064	0.733	11.8	1191	210	**283**	0.635
In	<0.146	0.026	0.313	2.03	**1**	0.001	0.006	11.3	0.419	0.390	**2**	0.260
Sn	4.97	4.96	0.084	146	**39**	0.125	1.039	118	95.9	85.9	**60**	5.02
Sb	1.53	0.11	0.336	2.69	**1**	0.027	0.111	22.1	3.82	4.79	**6**	0.655
Te	66.1	161	36.2	60.0	**81**	3.26	39.6	155	163	41.7	**80**	53.3
W	1.46	1.49	0.111	8.55	**3**	0.0416	0.405	30.2	3.06	0.84	**7**	2.79
Re	<0.26	1.45	0.79	0.43	**1**	0.0129	0.259	2.05	2.28	0.467	**1**	0.289
Os	2451	7771	34.4	651	**2727**	49.4	79.3	266	140	69.5	**121**	20.7
Ir	1667	1533	19.7	367	**897**	67.9	40.1	100.56	86.1	36.5	**66**	7.20
Pt	1722	1979	26.2	314	**1010**	2.75	54.4	46.8	68.8	9.08	**36**	35.4
Au	34.7	2.17	1.01	47.7	**21**	0.039	13.7	126	1345	0.85	**297**	40.8
Pb	6.38	4.63	20.0	105	**34**	0.619	7.83	74.9	81.9	33.1	**40**	2.80
Bi	<0.39	0.475	1.22	29.0	**10**	0.363	1.16	9.45	141	10.3	**33**	0.587
Re/Os	0.0001	0.0002	0.0230	0.0007	**0.0060**	0.0003	0.0033	0.0077	0.0163	0.0067	**0.0069**	0.0140
Os/Pt	1.4	3.9	1.3	2.1	**2**	17.9	1.5	5.7	2.0	7.7	**7**	0.6

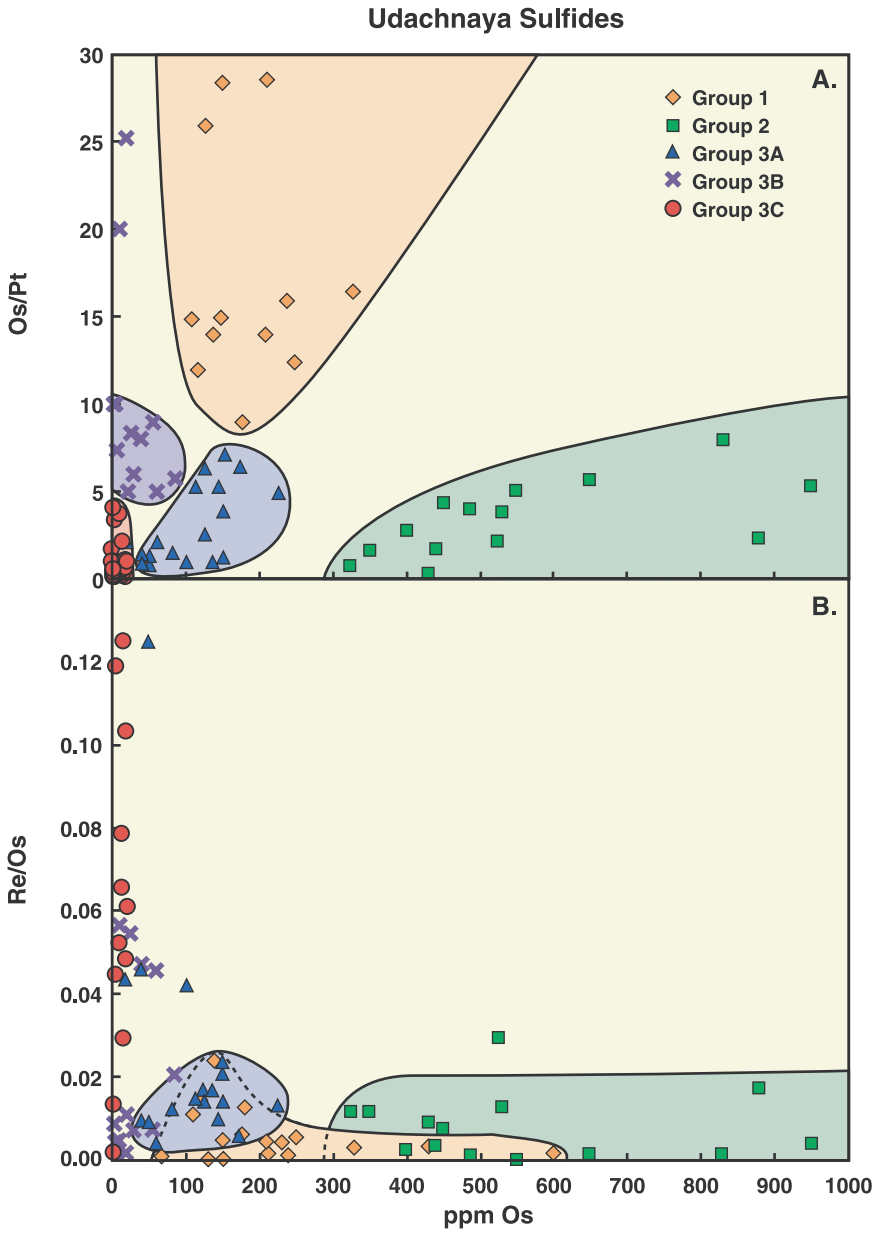

Figure 3. Re-Os-Pt data for sulfides analyzed by LAM-MC-ICPMS. Data from Table 3. (a) Os-Pt relationships of sulfide inclusions, showing defined populations. (b) Re-Os relationships of sulfide inclusions.

nants of sulfide, and these typically were near the rims of the original grains. Many of these analyses are therefore higher in Cu than the bulk of the sulfide, and some contain Pt nuggets not detected in the MC-ICPMS analysis.

[23] Group 1 sulfides show flat patterns (Figure 4a) between Os and Rh, and depletion in Pt and Pd; in half of the analyses Pt shows a small negative anomaly relative to Rh and Pd. Group 2 sulfides (Figure 4b) show a variety of patterns resulting in low Os/Pt; the most common has a steep negative slope and a pronounced positive Pt anomaly. Two samples (S50, S64–5) show gently sloping patterns with low Os/Pt but high Os/Pd. Sulfides from Groups 3A and 3B (Figure 4c) show essentially flat PGE patterns with small negative Pt anomalies. Sulfides from Group 3C (Figure 4d) show patterns

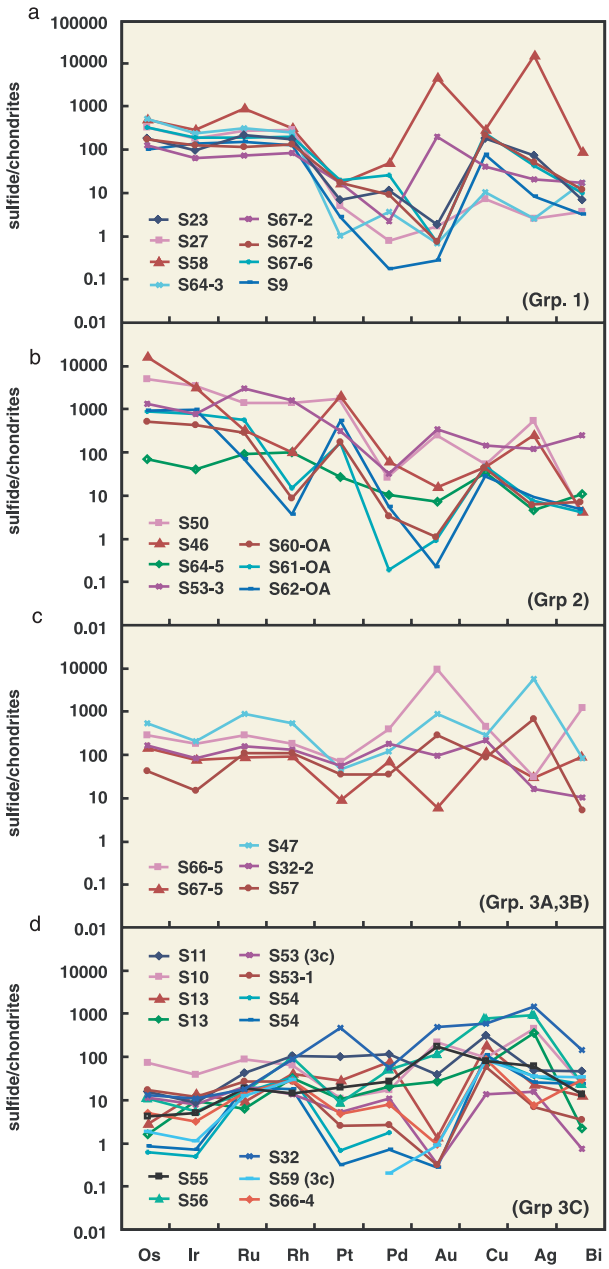

Figure 4. Trace element patterns of sulfide inclusions analyzed by LAM-ICPMS. Data from Table 3. (a) Group 1. (b) Group 2. (c) Groups 3A, 3B. (d) Group 3C.

with overall gently positive slopes, similar to those described by *Alard et al.* [2000] from interstitial sulfides in many spinel-peridotite xenoliths.

[24] The data for other trace elements show wide variability between samples, and between replicate analyses of individual grains, suggesting that individual trace elements are strongly partitioned among the several coexisting phases in each sulfide (Figure 2). Elements such as Au, Mo and Ag are concentrated in micronuggets, as seen in the time-resolved analysis (TRA) traces of individual phases. This heterogeneity tends to obscure broader differences among the different sulfide groups. However, the Group 3C inclusions have lower mean contents of most trace elements (other than Co) than the other groups. Zn, Se, Cd, Sn, Te and Pb are, on average, higher in Group 2 and Group 3A sulfides than in Groups 1 and 3C, which suggests that Groups 2 and 3A may be related and differ mainly in their total PGE contents (Figure 3).

4.2. Isotopic Data

[25] T_{RD} and T_{MA} model ages for most sulfides of Groups 1, 2 and 3A are >2.5 Ga; the mean 2σ uncertainty on these model ages, considering only the analytical uncertainties on $^{187}Os/^{188}Os$ and $^{187}Re/^{188}Os$, is ±0.1 Ga (Table 3). Several sulfides in Groups 3A and 3B give Proterozoic model ages. However, most sulfides from these groups, and all but one from Group 3C, have $^{187}Os/^{188}Os$ above the present-day CHUR value ($\gamma Os = 80–500$). Most inclusions with $^{187}Os/^{188}Os$ > CHUR also have $^{187}Re/^{188}Os$ < CHUR (i.e., < 0.4), and therefore also give negative T_{MA} model ages, but some have high Re/Os and give T_{MA} model ages that range from 3.9 to 11.6 Ga. The negative model ages, and ages greater than the age of the Earth, both demonstrate the presence of unsupported radiogenic Os in the sulfides, and require at least a two-stage evolution, with an early residence in a reservoir with Re/Os >CHUR. The spectrum of model ages that could in principle be considered geologically reasonable (i.e., 0–4 Ga) is shown in Figure 5.

[26] Six sulfide inclusions (23, 36-2, 53, 54, 65-4 and 67-2; Table 2) were large enough to allow reanalysis of their Os isotope composition following repolishing. Except for grains 23 and 65-4, the first analysis in each case represents the outer part of the inclusion, and the later analysis (or analyses, in the case of 67-2) represents the inner part of the grain. The two analyses of 65-4 are not significantly different; in the other cases the $^{187}Os/^{188}Os$ of the

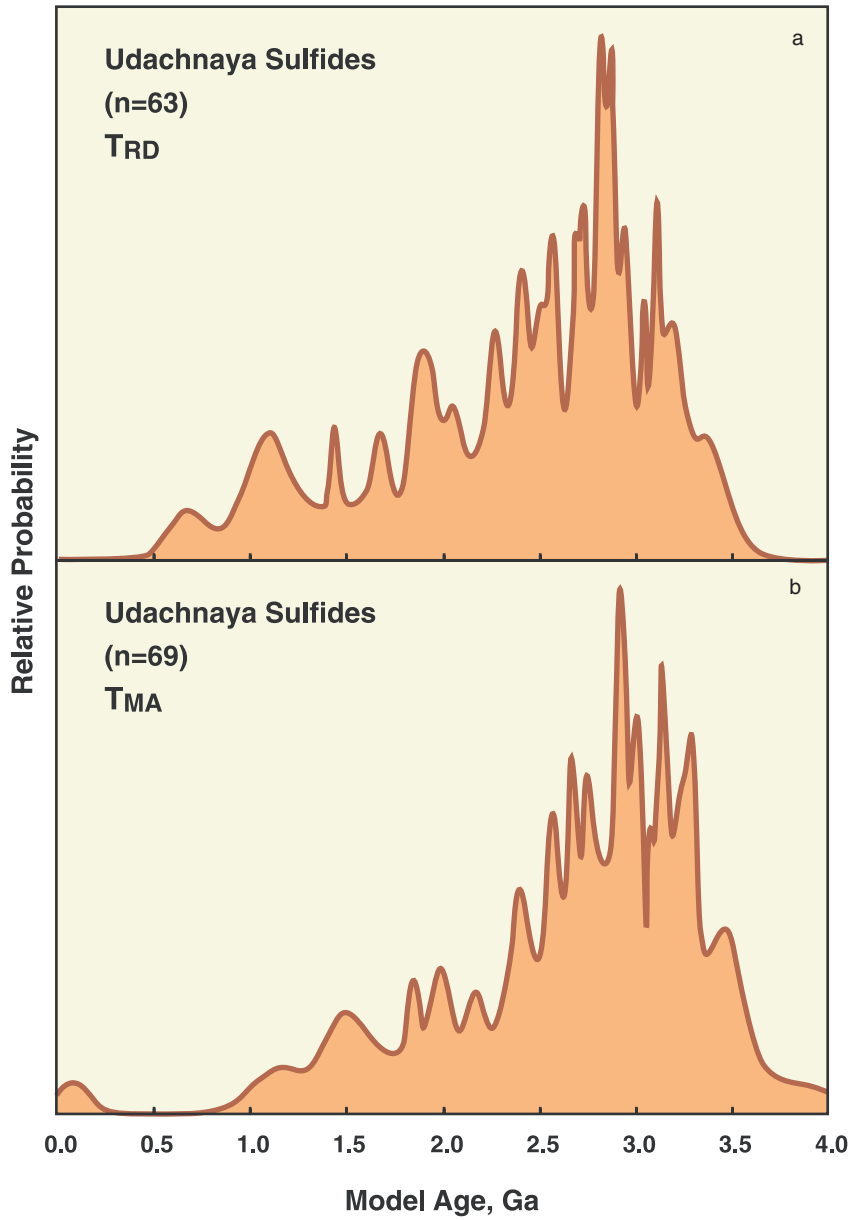

Figure 5. Cumulative probability plots [*Ludwig*, 2000] of model age data (Table 3). (a) T_{RD}; (b) T_{MA}.

interior is lower than that of the rim. In four examples, $^{187}Re/^{188}Os$ of different analyses is similar within error; in grains 53 and 54 it is higher in the rims of the grains. Two adjacent analyses of the interior of grain 67-2 (67-2B, 67-2C), performed in separate runs, are identical in terms of Re/Os and $^{187}Os/^{188}Os$. The third "interior" analysis, taken after further repolishing and LAM-ICPMS analysis (67-2D), has lower $^{187}Os/^{188}Os$. The differences in Re/Os and $^{187}Os/^{188}Os$ between different parts of single grains do not yield meaningful isochronous relationships; all "ages" are $\geq$4.5 Ga and have unrealistic initial ratios. Grains 53 and 54 are Group 3C sulfides with wide chalcopyrite rims (Figure 2). The higher Re/Os and $^{187}Os/^{188}Os$ in their outer parts suggest that Re is concentrated in these rims, as deduced by *Richardson et al.* [2001] for sulfide inclusions in diamonds. The isotopic heterogeneity observed in these large grains may reflect ingrowth of radiogenic ^{187}Os in their rims (which will tend to

have higher Cu contents and Re/Os), and its slow inward diffusion, over the ca 360 Ma since kimberlite eruption and the exsolution of the sulfides.

[27] Multiple sulfide inclusions have been analyzed in 10 olivine grains, including 3 in Ud-Ol-64, 4 in Ud-Ol-65 and 6 each in Ud-Ol-66 and Ud-Ol-67. In some cases the different inclusions belong to the same group, and are similar in isotopic composition (e.g. Ud-Ol-26, Ud-Ol-43, Ud-Ol-64). In the other cases, sulfides of different groups coexist within single olivine grains. Ud-Ol-9 contains one Group 1 and one Group 3A sulfide, with different T_{MA} (2.67, 3.07 Ga). Ud-Ol-66 contains two Group 3A sulfides with similar model ages (T_{MA} = 2.92 Ga, 2.96 Ga), but also contains four Group 3C sulfides with widely varying isotopic compositions and Re/Os ratios. Ud-Ol-67 contains one sulfide (67-2) which classifies as Group 1 or Group 3A in different analyses, four 3A and two 3C grains. with much more radiogenic Os-isotope compositions.

[28] In most cases combinations of the different sulfides within a single olivine cannot yield Re-Os isochrons with meaningful ages and initial ratios. This strongly suggests that the inclusions represent trapping of different generations of sulfides in one olivine grain. However, inclusions 66-3, 66-5 and 66-6, which have the highest Os contents among the sulfides in this olivine grain, yield an isochron age of 2786 ± 890 Ma (IR = 0.1069), which may suggest a cogenetic relationship among these sulfides of different groups (3A, 3C).

5. Discussion

[29] The data presented above raise a major question: which of the model ages derived from these sulfides represent real mantle depletion events? The unsupported radiogenic Os of many Group 3 sulfides requires a multistage evolution, and their existence implies that other samples also could have multistage histories and yield plausible, but still spurious, ages. In the discussion below, we attempt to place the interpretation of the sulfide data on a firmer basis, and to derive criteria for recognizing the model ages that are most likely to be meaningful.

5.1. Origin of Sulfide Populations

[30] Experimental studies of sulfide liquids [*Li et al.*, 1996; *Barnes et al.*, 1997, 2002; references therein] show that they evolve by fractional crystallization of MSS solid solutions. The melting of such sulfide compositions between 900–1100°C is incongruent, leaving a MSS as the residual phase; this MSS becomes progressively poorer in Ni and Cu as melting progresses. *Li et al.* [1996] and *Barnes et al.* [1997] have summarized new and existing experimental data on the partitioning of Cu, Ni and PGEs between MSS and sulfide liquids. They show that Ir (and by inference Os) are strongly partitioned into the MSS, whereas Cu, Pt and Pd are partitioned into the coexisting melt (Figure 6a). Under sulfur-undersaturated conditions, MSS and a range of alloy phases may coexist with sulfide liquid; the alloy phases strongly concentrate Ir and Pt, relative to Rh and Pd [*Li et al.*, 1996; *Barnes et al.*, 1997]. In these experiments, which were doped with PGEs at percent levels, the exact values of $D^{MSS/Liq}$ for each element vary with the S content of the system. However, experiments at lower PGE concentrations suggest little variation of D values with S content [*Balhaus et al.*, 2001].

[31] On the assumption that a Primitive Mantle source rock has a chondritic PGE pattern, and that the PGEs are concentrated in the primitive sulfide phase, such primitive sulfides would be expected to have relatively low Os contents and chondritic relative abundances of the PGEs. The high Os contents of Group 1 and Group 2 sulfides, and the PGE patterns shown in Figures 4a–4d, are not consistent with primitive sulfides, and strongly suggest that these sulfide inclusions in olivine represent MSS phases, residual after partial melting. The flat PGE patterns of Group 3A sulfides (Figure 4c) are consistent with their being primitive sulfides, but their high Os contents are not (see below). Conversely, the low Os contents and high Cu contents of the Group 3C sulfides (and the PGE data on Group 3C sulfides; Figure 4d) suggest that

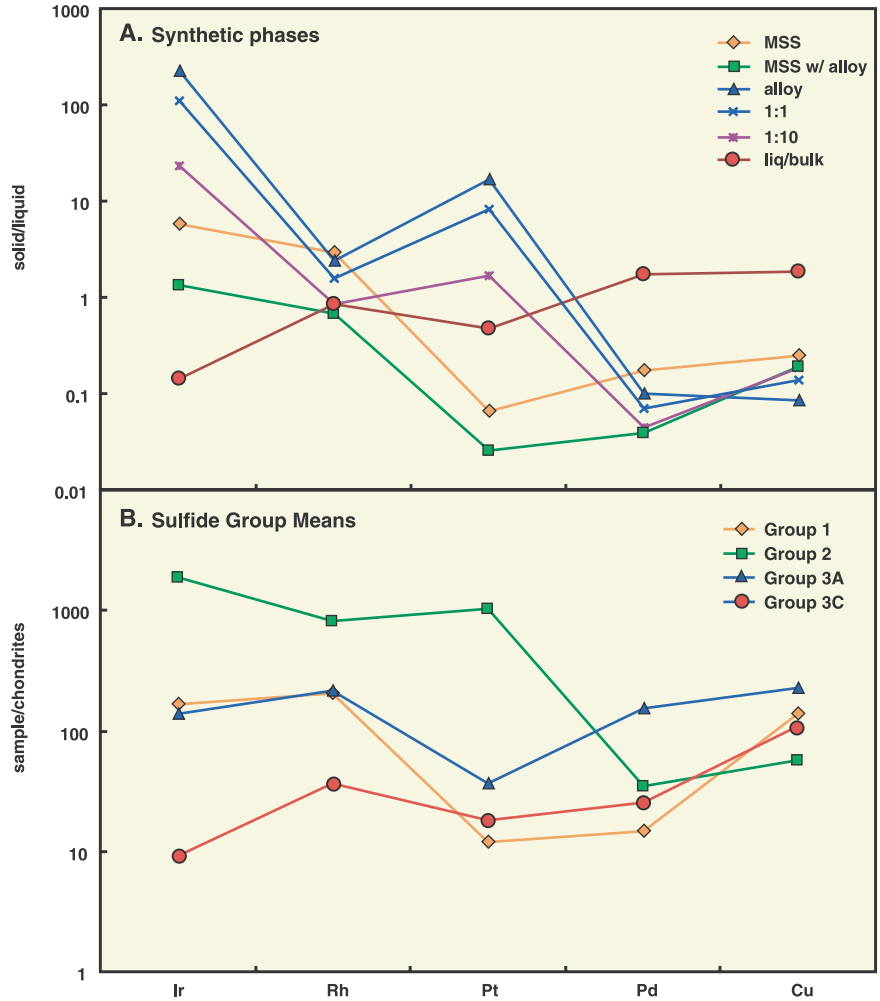

Figure 6. PGE patterns for (a) synthetic MSS and alloys and (b) group averages of sulfide inclusions.

they represent trapped melts, or MSS crystallized from such melts after separation from residual MSS [*Alard et al.*, 2000].

[32] To examine the possible origins of the different sulfide groups, we have modeled the Os and Pt contents of MSS residual from progressive batch melting of a Primitive Mantle source; modeling parameters are given in Table 5. We have used the partition coefficients for Ir (as proxy for Os) and Pt suggested by *Li et al.* [1996] and *Barnes et al.* [1997] for sulfur-saturated and sulfur-undersaturated melting; these are similar to the values reported by *Balhaus et al.* [2001]. We are not aware of reliable experimental data on Re partitioning. Given the very low Re/Os of the Group 1 and Group 2 MSS, we therefore have adopted a value for $D_{Re}^{mss/melt}$ (0.02) consistent with Re being incompatible in MSS; as seen below, this produces results consistent with our observations. The Primitive Mantle source is assumed to contain 238 ppm S, corresponding to ca 680 ppm sulfide, and all Os, Pt and Re are assumed to reside in this sulfide prior

Table 5. Parameters for Modeling of MSS and Alloy Compositions

	Depleted Mantle	Primitive Sulfide	$D^{mss/liq}$	$D^{alloy/liq}$
	ppm	ppm		
Os	0.00343	5.4	4	300
Pt	0.00707	11.8	0.03	20
Re	0.00027	0.45	0.02	0.002
S	238	35%		

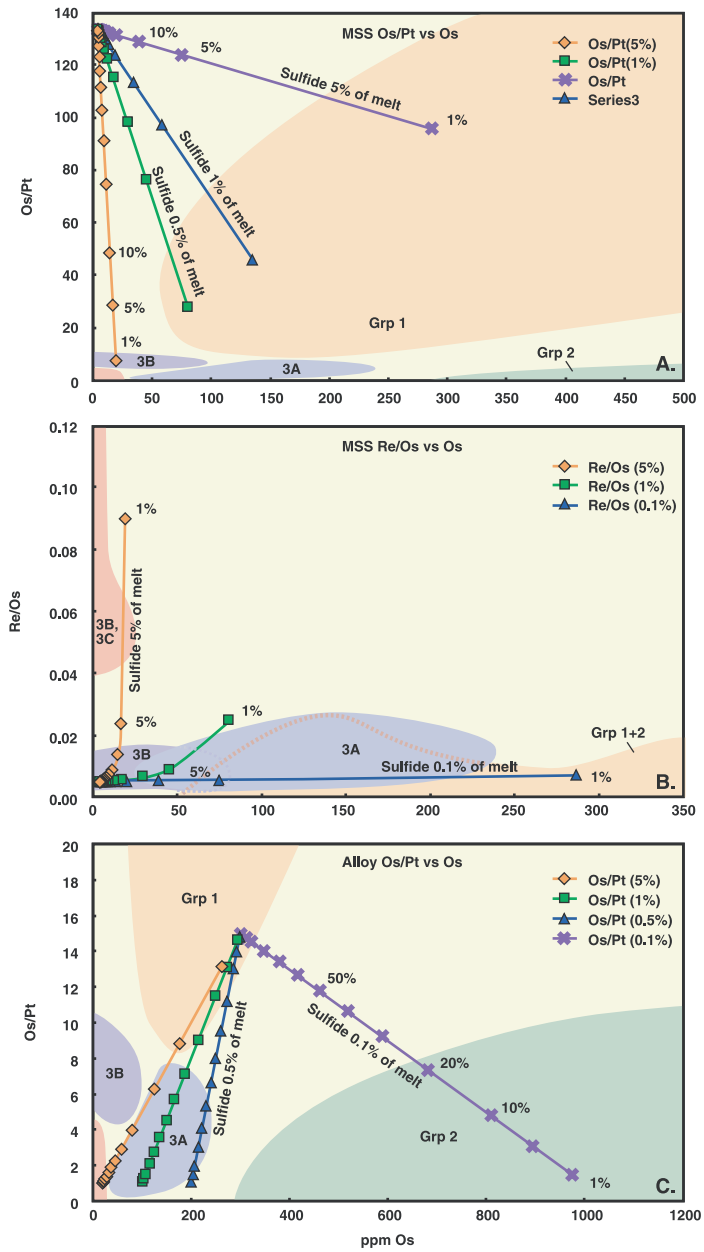

Figure 7. Modeled compositions of MSS and alloy phases, produced by melting of a Primitive Mantle composition. Modeling parameters given in Table 5. (a) Os-Pt relationships in MSS, with fields of sulfide groups from Figure 3a. (b) Re-Os relationships in MSS, with fields of sulfide groups from Figure 3b. (c) Os-Pt relationships in alloy phase, with fields of sulfide groups from Figure 3a.

to melting. The modal percent of sulfide contributing to the melt has been varied from 0.1% (i.e. sulfide melting roughly twice as fast as the silicate matrix) to 5% (i.e. very rapid melting of sulfide relative to silicate).

[33] The Os and Pt contents and Os/Pt and Re/Os ratios produced in residual MSS at different degrees of melting under sulfur-saturated conditions are shown in Figure 7. Maximum Os contents drop from 290 ppm to 20 ppm as the rate of sulfide melting or the degree of total melting is increased, while Os/Pt ratios drop from ca 95 to < 10 (Figure 7a). Re/Os is low (0.007–.005) in the MSS produced at low rates of sulfide melting, and similar to the mean Re/Os

of the Group 1 and 2 sulfides (Figure 7b). Higher Re/Os (to 0.1) can be produced by high modal proportions of sulfide melting, but few of the modeled MSS have Re/Os >0.02.

[34] It is apparent from these models that MSS with the high Os contents and low Os/Pt seen in the Group 2 sulfides cannot be produced by single-stage melting of a Primitive Mantle sulfide (Figure 7a). However, alloy phases produced at low rates of sulfide melting will have both high Os contents and low Os Pt, similar to those of Group 2 sulfides (Figure 7c).

[35] The Group 2 sulfide inclusions obviously are not alloys, but they do contain discrete micronuggets rich in Pt. They therefore may represent very fine-grained mixtures of alloy phases and MSS. Group 1 MSS have negative Pt anomalies (Figure 6b), like the MSS produced in experimental charges at both sulfur-saturated and sulfur-undersaturated conditions (Figure 6a). The PGE patterns of Group 2 sulfides, in contrast, show a positive Pt anomaly, or a weak negative anomaly (Figure 6b). A positive Pt anomaly also is observed in experimentally produced alloy phases (Figure 6a). Because Pt is so strongly concentrated in the alloy phase, even a small proportion of the alloy in the MSS phase will impart a positive Pt anomaly to a mixed phase, which also will have a high Os content and a low Os/Pt ratio. For example, mixtures of 10% alloy + 90% MSS (Figure 6a) have overall PGE patterns similar to those of Group 2 sulfides, with high Ir, a positive Pt anomaly, and low Pd and Cu.

[36] We therefore suggest that the Group 2 sulfides originally consisted of a mixture of MSS and an alloy phase, residual from small degrees of partial melting of a Primitive Mantle sulfide under sulfur-undersaturated conditions. Subsequent remelting, quenching and exsolution (Figure 2) probably has modified these inclusions to the point that petrographic evidence for this earlier history, other than the existence of Pt-rich micronuggets, reflecting a high metal/sulfur ratio, has been lost. In this analysis, the extremely high Os contents of Group 2 inclusions would reflect low degrees of melting. This is consistent with both their high Cu and Ni contents, compared to Group 1 sulfides, and their concentration in the lowest-Fo olivines in our sample set (Table 3).

[37] If Group 1 and Group 2 sulfides represent MSS (±alloy phases) derived from low degrees of partial melting, the Group 3 sulfides require another explanation. On the basis of their PGE patterns (Figure 4d, Figure 6b), Group 3C sulfides are interpreted as trapped melts, or as MSS crystallized from partial melts high in Cu and low in Os, and with low Os/Pt. Most Group 3A and Group 3B sulfides have Os contents too high to be consistent with their being melts, but Cu contents too high to be consistent with MSS crystallization except perhaps from very Cu-rich melts. On the other hand, if their flat PGE patterns (Figure 4c) are to be interpreted as reflecting a primitive nature, the sulfide content of the Primitive Mantle would have to be roughly 60 ppm, or 1/10 currently accepted estimates. We suggest that this anomalous combination of features may result from interaction between residual sulfides and younger sulfide melts, and believe that this interpretation is supported by the isotopic data (detailed in section 5.2).

5.2. Origin and Evolution of Sulfide Inclusions

[38] The sulfides observed here were not generated inside olivine crystals; the existence of isolated residual MSS crystals implies the existence of pathways for the escape of the coexisting melts, and the presence of possible melt inclusions (some Group 3C sulfides) implies movement along grain boundaries or through cracks (such as those evidenced by planar veins in many mantle xenoliths). We suggest that sulfide liquids could penetrate olivine crystals along cracks, and both melts and crystallizing MSS could be trapped by necking-down processes like those that produce fluid inclusions in crustal rocks. *Alard et al.* [2000] distinguished ''enclosed'' sulfides (chemically similar to Groups 1 and 2) from ''interstitial'' sulfides (chemically similar to Group 3C) on the basis of observations in relatively fine-grained xenoliths. The occurrence of both types as enclosed sulfides in the Udachnaya samples, and within the same olivine grain in some cases, suggests that grain-

boundary migration (grain growth) in initially finer-grained rocks has produced the large olivine crystals sampled here, and has been important in trapping sulfide inclusions.

[39] The presence of more than one generation of sulfide in several of the analyzed grains suggests that this process has occurred several times, first trapping the oldest residual MSS (Groups 1, 2) and later trapping sulfide melts moving along grain boundaries and through cracks, or MSS crystallized from them. These processes offer the possibility of reaction between migrating sulfide melts (or other fluids carrying Os, Pt and Re) and pre-existing MSS, to produce a range of sulfide types including ancient residual MSS (Groups 1, 2), sulfide melts or MSS crystallized from them (Group 3C) and pre-existing MSS that have reacted with younger melts (Groups 3A and 3B, and some Group 1 and 2 sulfides). These reacted sulfides may be recognizable by their higher Cu and higher Re/Os ratios.

5.3. A Mixing Model and the Interpretation of Model Ages

[40] A plot of T_{MA} versus T_{RD} (Figure 8a) shows that some of the Group 3 sulfides scatter into the quadrant with ($T_{MA} > 0$, $T_{RD} < 0$); in whole rock xenolith studies this pattern commonly is interpreted as reflecting the addition of Re to the sample near the time of eruption. These Group 3C sulfides may have been introduced into the lithosphere shortly before kimberlite eruption. However, other Group 3 sulfides define a trend extending into the quadrant with ($T_{MA} < 0$, $T_{RD} < 0$), implying a multistage growth in which the Re/Os of the earlier stage(s) was less than that of the analyzed sample. In whole rock studies this is commonly ascribed to a recent loss of Re; however, it is difficult to see a mechanism for causing Re loss in individual sulfide inclusions within olivine.

[41] A plot of T_{MA} versus $^{187}Re/^{188}Os$ (Figure 8b) shows these two trends in another perspective. A broad scatter of data from Group 3C sulfides (extending well outside the range of the figure) shows a trend of increasing T_{MA} with increasing Re/Os, as would be expected from addition of Re to samples with $^{187}Os/^{188}Os <$ CHUR. This positive correlation also is observed in whole rock Re-Os data for peridotite xenoliths from both Siberia and South Africa [*Pearson et al.*, 1995a, 1995b, 1997; *Carlson et al.*, 1999], where it has been interpreted as the effect of young Re addition. These Group 3C sulfides may be the material by which such Re addition occurs.

[42] However, many of the other data points, including some Group 2 as well as Group 3 sulfides, define a negative trend between sulfides with high γOs and low Re/Os (Groups 1 and 2), and others with very high γOs and relatively modest Re/Os (<CHUR). As noted above, the trace element systematics of the Group 3 sulfides suggest a mixing process, in which Group 3A and 3B sulfides have acquired a hybrid PGE pattern by reaction between residual sulfides and sulfide melts more similar to some Group 3C sulfides. We suggest that the Re-Os data may be explained by a similar mixing probess.

[43] The existence of sulfides with $^{187}Os/^{188}Os >$ CHUR (up to $\gamma Os = 400$), but $T_{MA} > 4.5$ Ga, requires a two-stage evolution involving an older source that has Re/Os higher than most estimates for the convecting mantle, and presumably must reside within the lithosphere. An appropriate candidate for this source is represented by eclogite xenoliths from Udachnaya, the Re-Os systematics of which have been studied by *Pearson et al.* [1995b, 1995c]. These eclogite xenoliths scatter about a 2.9 Ma Re-Os isochron; four of them define a 3.2 Ga isochron. They have a mean Os content of 0.1 ppb and a mean $^{187}Re/^{188}Os = 99$ (range 12–211), and are capable of generating extremely high $^{187}Os/^{188}Os$ within 10–100 Ga after their separation from the primitive mantle. Similar high Re/Os ratios and very radiogenic Os have been described from inclusions of eclogitic (low-Ni [*Bulanova et al.*, 1996]) sulfide in African diamonds [*Pearson et al.*, 1999; *Shirey et al.*, 2001]. While PGE patterns are not available for the Udachnaya eclogites, we assume that they have the low Os/Pt characteristic of most basaltic rocks.

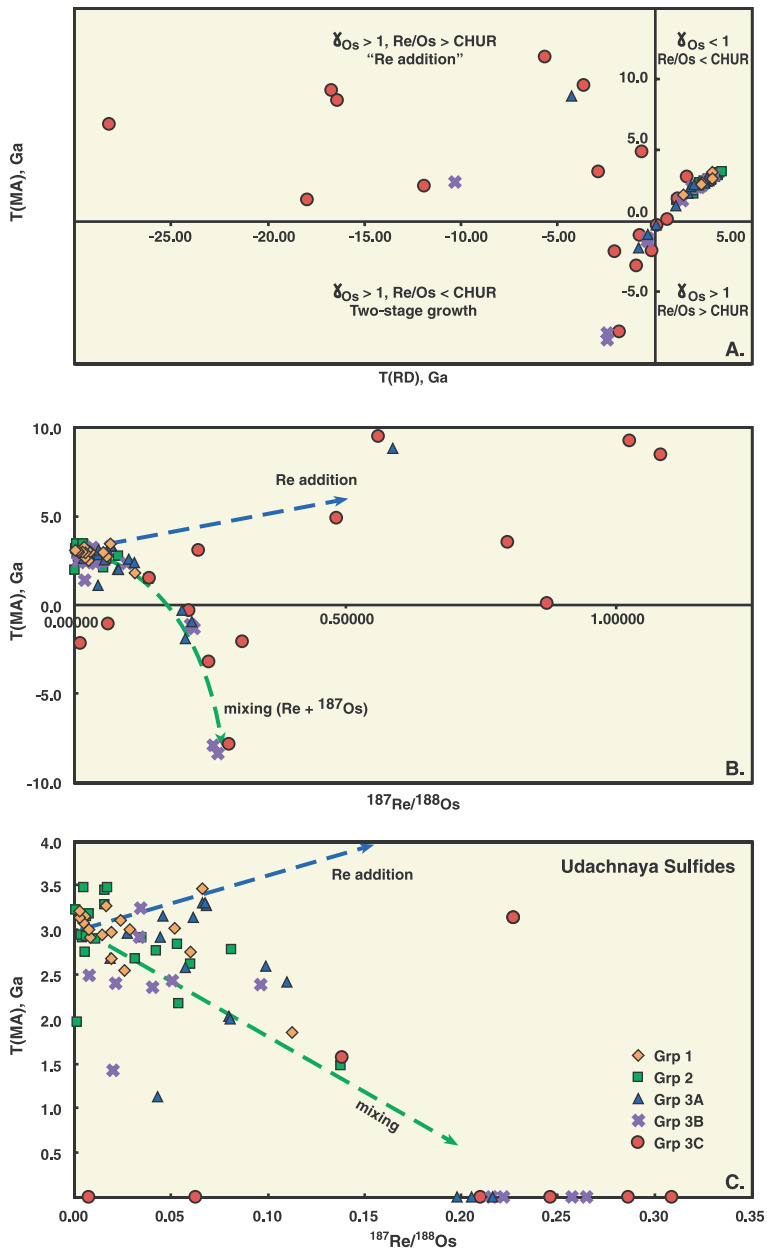

Figure 8. (a) T_{MA} versus T_{RD}, showing scatter of some Group 3C sulfides into upper left quadrant, and others into lower left. (b) T_{MA} versus $^{187}Re/^{188}Os$, showing the broad positive trend produced by late Re addition, and the better-defined negative trend inferred to result from addition of sulfide melts derived from eclogites. (c) Expanded view of Figure 8b. Samples with negative T_{MA} are plotted on the X axis.

[44] If small-volume melts were produced by partial remelting of these eclogites within a few hundred Ma after their initial formation, and penetrated into the surrounding peridotite wall rocks, they could precipitate sulfides resembling the Group 3C inclusions, and produce the Group 3B–3C sulfides by reaction with pre-existing Group 1 and Group 2 sulfides. The degree to which this reaction would modify the Os isotope composition and Re/Os of the pre-existing MSS would depend on the Os content of the MSS and the volume ratio of MSS to fluid. Such mixing may be recorded by the heterogeneity in Os isotope composition (±Re/Os) observed by the sequential

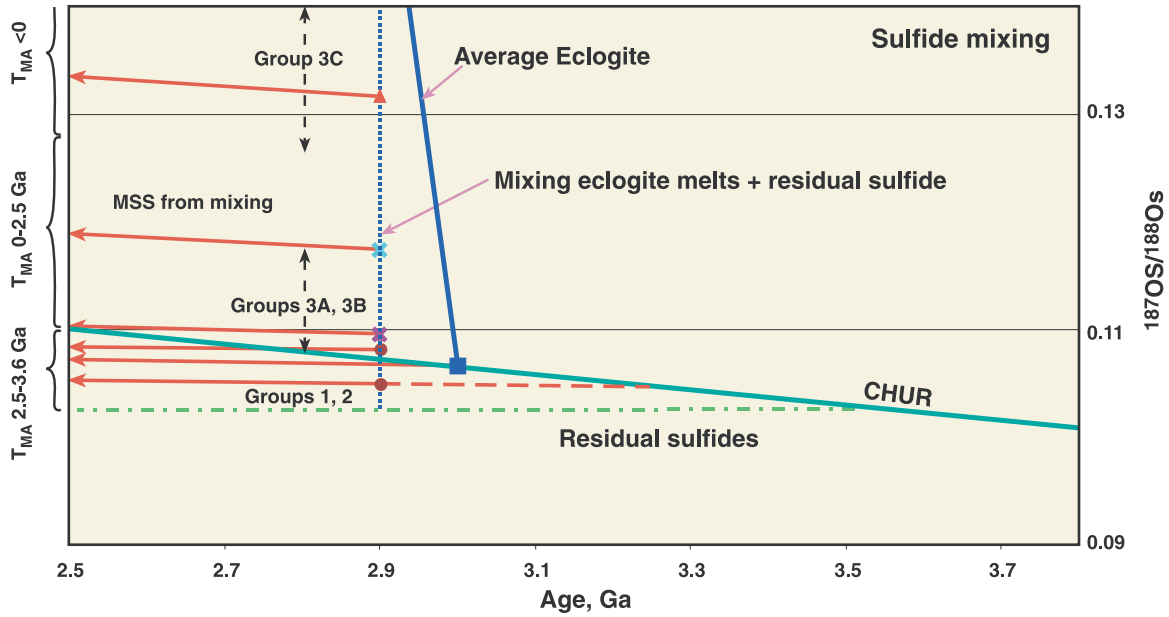

Figure 9. Re-Os systematics of a lithosphere formed at 3.5 Ga and intruded by eclogites at 3.0 Ga, which are remelted at 2.9 Ga to produce low-volume sulfide-bearing melts. Reaction between residual sulfides and sulfide melts produces a range of $^{187}Os/^{188}Os$, and a correlated increase in Re/Os, depending on the Os contents of residual sulfides melts. Mixed sulfides give a range of spurious younger model ages.

sectioning of several sulfide inclusions (23, 53, 54 and 67-2; Table 3). The mixing model is illustrated in Figure 9.

[45] If this model is a correct explanation of the Re-Os systematics of the Udachnaya sulfide inclusions, it implies that only those sulfides with low Re/Os are likely to yield realistic T_{MA} model ages. The Re-Os modeling above indicates that most residual MSS derived from melting of mantle peridotite will have Re/Os < 0.015 ($^{187}Re/^{188}Os$ < 0.07; Figure 3b). If we adopt this cutoff value, we obtain the spectrum of T_{MA} model ages shown in Figure 10.

[46] A Re-Os isochron plot for all of the data with $^{187}Re/^{188}Os$ < 0.4 shows a broad trend with a slope corresponding to an age of ca 6 Ga, which is clearly a mixing line (Figure 11a). The data for Group 1, 2 and 3A inclusions, and the diamond-inclusion data of *Pearson et al.* [1999] are plotted in Figure 11b. The use of in situ analytical data to derive Re-Os isochrons faces one major problem: the thin chalcopyrite rims of the sulfides are likely to have higher Re/Os than the bulk of the inclusion [*Richardson et al.*, 2001]. These rims were formed during exsolution immediately after eruption and quenching, and low temperatures would hinder isotopic equilibration between rim and core. As noted above, this may be reflected in the isotopic differences observed between rim and core of some large sulfide grains. To use the analyzed Re/Os ratios with any precision, it therefore is necessary to assume either that the entire inclusion has been sampled by the laser (true in most cases) or that isotopic equilibration between rim and core has not occurred. The latter assumption is supported by the isotopic similarity of multiple analyses of several of the larger sulfide grains.

[47] Fifteen of the low-Re/Os points scatter about a reference isochron for CHUR at 3.2 Ga, and 20 points scatter about a 2.9 Ga reference isochron; these groupings reflect major peaks in the T_{MA} spectrum (Figure 10). Several points with low Re/Os fall below the 3.2 Ga reference line, and these are interpreted as representing more ancient events. A cluster of points with $^{187}Re/^{188}Os$ = 0.2–0.3, and some with low $^{187}Re/^{188}Os$, scatter about a 2.9 Ga reference line with a high initial $^{187}Os/^{188}Os \approx$

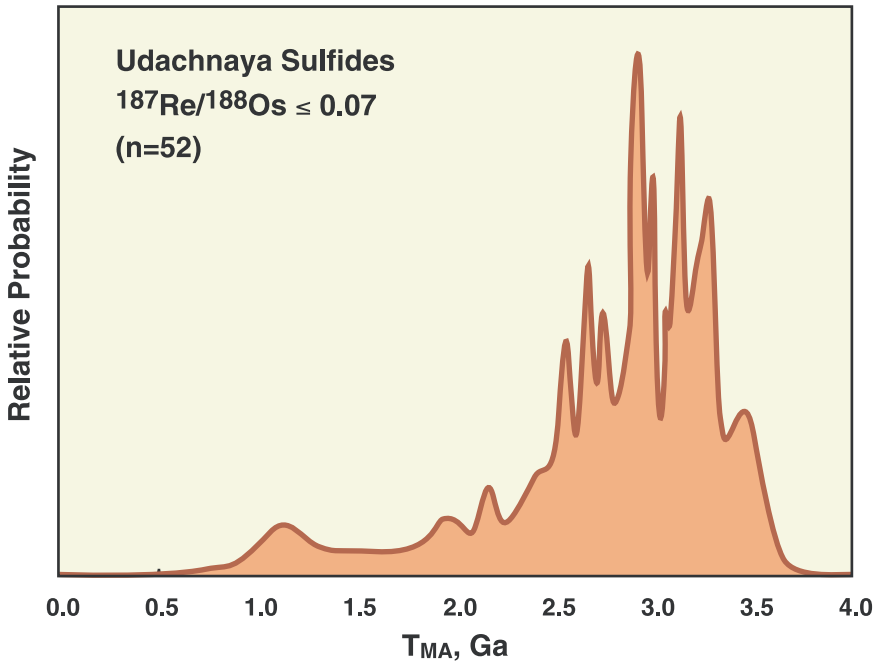

Figure 10. T_{MA} model ages of sulfide inclusions with $^{187}Re/^{188}Os \leq 0.07$, corresponding to the range of Re/Os expected in primary MSS phases derived by melting of Primitive Mantle (Figure 7B).

0.118. None of these points lie along the "Re-addition" array in Figures 8a–8c, and we suggest they might represent the radiogenic component derived from the eclogites. Similar $^{187}Os/^{188}Os$ ratios characterized several of the eclogites analyzed by *Pearson et al.* [1995b, 1995c] at 2.9–3.0 Ga. Several points with $^{187}Re/^{188}Os = 0.05–0.15$ lie on a trend toward the cluster of high-Re/Os points, reflecting the inferred addition of both radiogenic Os and Re. This mixing trend is equivalent to the slope of the regression line shown in Figure 11a.

5.4. Comparison With Previous Data

[48] *Pearson et al.* [1995a] reported Re-Os data for 18 peridotite xenoliths from Udachnaya, and for olivine separated from two of these. Most of these samples have high $^{187}Os/^{188}Os$ ($\geq$0.12) and very high $^{187}Re/^{188}Os$ ($\geq$2). The samples scatter about a 489 Ma reference line with a high initial $^{187}Os/^{188}Os$ (0.112); this is distinct from the overall array defined by the sulfide-inclusion data reported here (Figure 11b), and suggests addition of Re to the whole rocks shortly before eruption of the Udachnaya kimberlite at ca 360 Ma [*Pearson et al.*, 1995a]. *Pearson et al.* [1995a] have argued from Sm-Nd systematics that the mantle beneath Udachnaya underwent a significant metasomatic event at this time; the data presented here suggest that some of the Group 3C sulfides may have been introduced then as well, providing the "Re enrichment". The occurrence of these sulfides as inclusions in large olivine grains implies ongoing recrystallization, consistent with the model of *Pearson et al.* [1995a].

[49] Four of the peridotite samples analyzed by *Pearson et al.* [1995a] have T_{MA} model ages between 2.2 and 3.9 Ga, using the model-age parameters adopted here (footnote, Table 2); most T_{RD} model ages range from 1–3 Ga, comparable with the range found in this study (Figure 5a). However, comparison with the data from the enclosed sulfides suggests that few of these model ages are geologically meaningful. The sulfide data imply that the isotopic composition of Os extracted from the whole rock samples reflects not only Re addition near the time of kimberlite eruption, but the mixing of several sulfide generations with very different Os isotope compositions. This point is emphasized by the occurrence of several genera-

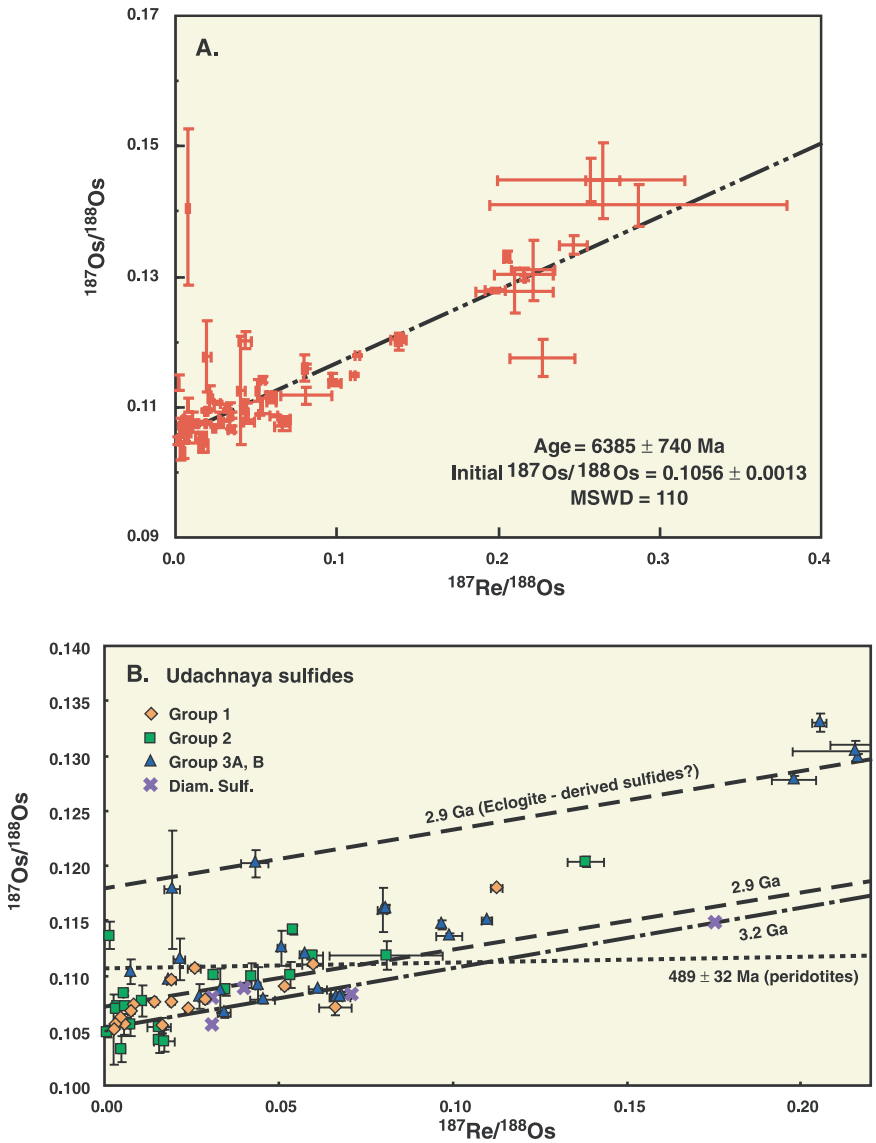

Figure 11. Re-Os isochron plots. (a) All sulfides with $^{187}Re/^{188}Os \leq 0.4$; regression line is interpreted to reflect mixing between residual sulfides and eclogite-derived sulfides at ca 2.9 Ga. (b) Sulfides of Groups 1, 2, and 3A, with reference lines for CHUR at 2.9 and 3.2 Ga, and for a postulated eclogitic component at 2.9 Ga. 489 Ma reference line passes through whole rock data of *Pearson et al.* [1995b]. Udachnaya diamond-inclusion sulfides are from *Pearson et al.* [1999].

tions of sulfide inclusions even within single olivine grains in our sample set (Table 2), and by the large differences in $^{187}Os/^{188}Os$ between two whole rocks and their separated olivines reported by *Pearson et al.* [1995a].

[50] The only sample analyzed by *Pearson et al.* [1995a] that satisfies the criteria suggested above is an olivine separate from a megacrystalline dunite, which has T_{RD} = 2.77 Ga and T_{MA} = 2.9 Ga, similar to data from many Group 1 and Group 2 sulfides reported here. Another olivine separate has $^{187}Os/^{188}Os$ = 0.24174, similar to values from several Group 3C sulfides in the present study. One whole rock sample has $^{187}Re/^{188}Os$ = 0.079, T_{RD} = 1.9 Ga and T_{MA} = 2.3 Ga; this sample lies above the 2.9 Ga CHUR reference isochron (Figure 11b).

[51] Five sulfide inclusions in Udachnaya diamonds [*Pearson et al.*, 1999] have $^{187}Re/^{188}Os$ = 0.031–0.175 and fall within the array shown in Figure 11b; their T_{MA} model ages range from 2.93–3.37 Ga, consistent with most of the data on low-Re/Os sulfides from this study (Figure 10). The PGE patterns of these inclusions [*Bulanova et al.*, 1996] indicate that they are Group 1 or Group 2 sulfides; their Os contents are 70–110 ppm, while Pt contents were below the detection of the proton microprobe (ca 50 ppm).

5.5. Formation of the SCLM Beneath Udachnaya

[52] On the basis of the data presented here, and the assumption that the formation of residual sulfides coincided with melt extraction from the peridotitic mantle, we suggest that much of the SCLM beneath the Udachnaya pipe was stabilized between 3.5 and 3.0 Ga ago by one or more major melt-extraction events. Eclogites were formed either by the intrusion of mafic melts, or by subduction of crustal basalts, between 3.2 and 2.9 Ga [*Pearson et al.*, 1995b, 1995c], and would rapidly have evolved highly radiogenic Os isotope compositions. To explain the range of observed Os isotope compositions in the enclosed sulfides, we suggest that partial remelting of these eclogites at ca 2.9 Ga produced melts with high $^{187}Os/^{188}Os$ and moderate Re/Os, which penetrated the surrounding mantle wall rocks and reacted to varying degrees with discrete grains of Os-rich MSS. The heat required for this melting event may also have produced depletion in some mantle peridotites, so that it is recorded in the Os isotope compositions of many enclosed sulfides. It is plausible that the 2.9 Ga event recorded by the eclogites dates the subduction and recrystallization of their basaltic protoliths, and their emplacement into the mantle root.

[53] The major peak of T_{MA} values around 2.9 Ga, and the scarcity of younger model ages, (Figure 10) suggests that this event signaled the end of major lithosphere formation in this area. Several individual inclusions with low Re/Os and $T_{MA} < 2.6$ Ga may represent new additions to the lithosphere, but we cannot exclude the possibility that these too reflect mixing of sulfide generations.

[54] This scenario is consistent with the limited data on crustal formation in the Daldyn terrane. These suggest a major crust-forming event around 3.0 Ga, and minor igneous activity related to the major terrane boundaries and associated with the amalgamation of the craton around 1.8–2.0 Ga [*Rosen et al.*, 1994]. Further data on the timing of both crust and mantle events will be required to investigate the detailed relationships between the two.

6. Conclusions

[55] Most, if not all, of the SCLM sampled in this reconnaissance study probably formed during the period 3.0–3.5 Ga, and lithosphere formation may have culminated in a major event at ca 2.9 Ga. There is little evidence in the Re-Os data for significant further additions to the lithospheric mantle after this time. Further detailed studies of sulfides from individual xenoliths will be required to determine if there is a relationship between age and depth in this lithospheric section.

[56] Comparison of these results with whole rock data on peridotite xenoliths suggests that measurement of geologically meaningful model ages on these rocks may only be possible through use of in situ techniques like those employed here. The analysis of separated olivine (or other silicates or oxides) containing sulfide inclusions can avoid most effects of recent Re addition, but also may be affected by mixing of several generations of sulfide. This mixing is demonstrated by the wide range of Os isotope compositions in sulfide inclusions from single olivine grains. The data from the sulfide inclusions show that Os is not immobile in the lithospheric mantle; sulfide mobility affects Re-Os systematics at all scales in cratonic lithospheric mantle, as well as in the off-craton situations described by *Alard et al.* [2002]. Even the analysis of single sulfide grains will require careful interpretation, based on the composition of the sulfides, but the in situ technique does remove several degrees of freedom that affect bulk-anal-

ysis techniques. Detailed studies of sulfide phases therefore promise greater insights into the evolution of the subcontinental mantle than has been possible previously.

Acknowledgments

[57] We thank Ashwini Sharma and Suzie Elhou for help with the LAM-ICPMS analyses, and Andy Burroughs of Nu Instruments for useful suggestions on ion-counter calibration. Sarah-Jane Barnes and Chris Ballhaus contributed very helpful discussions regarding the interpretation of experimental work. We also thank Olivier Alard and Sonja Aulbach for ongoing discussions about mantle sulfides and their interpretation. The manuscript was improved by a thoughtful review from Rick Carlson. Funding for this work was provided by an ARC Large Grant (WLG/SYO'R) and Macquarie University research grants. This is contribution #292 from the ARC National Key Centre for Geochemical Evolution and Metallogeny of Continents.

References

Alard, O., W. L. Griffin, J. P. Lorand, S. E. Jackson, and S. Y. O'Reilly, Non-chondritic distribution of the highly siderophile elements in mantle sulfides, *Nature*, *407*, 891–894, 2000.

Alard, O., W. L. Griffin, N. J. Pearson, J. P. Lorand, and S. Y. O'Reilly, New insights into the Re-Os systematics of subcontinental lithospheric mantle from in situ analysis of sulfides, *Earth Planet. Sci. Lett.*, in press, 2002.

Balhaus, C., M. Tredoux, and A. Spaeth, Experimental fractination of magmatic Fe-Ni-Cu-PGE sulfide melts: With application to the Sudbury igneous complex, paper presented at Eleventh Annual Goldschmidt Conference, Hot Springs, Va., 2001.

Barnes, S. J., E. Makovicky, M. Mackovicky, J. Rose-Hansen, and S. Karup-Moller, Partition coefficients for Ni, Cu, Pd, Pt, Rh and Ir between monosulfide solid solution and sulfide liquid and the formation of compositionally zoned Ni-Cu sulfide bodies by fractional crystallization of sulfide liquid, *Can. J. Earth Sci.*, *34*, 366–374, 1997.

Barnes, S. J., E. van Achterbergh, and E. Makovicky, Partitioning of Ni, Cu and PGE among monosulfide solid solution, sulphide liquid and metal alloys, *S. Afr. J. Geol.*, in press, 2002.

Boyd, F. R., A Siberian geotherm based on lherzolite xenoliths from the Udachnaya kimberlite, U.S.S.R, *Geology*, *12*, 528–530, 1984.

Boyd, F. R., N. P. Pokhilenko, D. G. Pearson, S. A. Mertzman, N. V. Sobolev, and L. W. Finger, Composition of the Siberian cratonic mantle: Evidence from Udachnaya peridotite xenoliths, *Contrib. Mineral. Petrol.*, *128*, 228–246, 1997.

Bulanova, G. P., W. L. Griffin, C. G. Ryan, O. Y. Shestakova, and S.-J. Barnes, Trace elements in sulfide inclusions from Yakutian diamonds, *Contrib. Mineral. Petrol.*, *124*, 111–125, 1996.

Carlson, R. W., D. G. Pearson, F. R. Boyd, S. B. Shirey, G. Irvine, A. H. Menzies and J. J. Gurney, Re-Os systematics of lithospheric peridotites: Implications for lithosphere formation and preservation, in *Proceedings of 7th International Kimberlite Conference*, edited by J. J. Gurney et al., pp. 99–108, Redroof Designs, Cape Town, 1999.

Gaul, O. F., W. L. Griffin, S. Y. O'Reilly, and N. J. Pearson, Mapping olivine composition in the lithospheric mantle, *Earth Planet. Sci. Lett.*, *182*, 223–235, 2000.

Griffin, W. L., F. V. Kaminsky, C. G. Ryan, S. Y. O'Reilly, T. T. Win, and I. P. Ilupin, Thermal state and composition of the lithospheric mantle beneath the Daldyn kimberlite field, Yakutia, *Tectonophysics*, *262*, 19–33, 1996.

Griffin, W. L., C. G. Ryan, F. V. Kaminsky, S. Y. O'Reilly, L. M. Natapov, T. T. Win, P. D. Kinny, and I. P. Ilupin, The Siberian Lithosphere Traverse: Mantle terranes and the assembly of the Siberian Craton, *Tectonophysics*, *310*, 1–35, 1999.

Hart, S. R., and G. E. Ravizza, Os partitioning between phases in lherzolite and basalt, in *Earth Processes: Reading the Isotopic Code*, *Geophys. Monogr. Ser.*, vol. 95, edited by A. Basu and S. R. Hart, pp. 123–134, AGU, Washington, D.C., 1996.

Lambert, D. D., J. G. Foster, L. R. Frick, D. M. Hoatson, and A. C. Purvis, Application of the Re-Os isotopic system to the study of Precambrian magmatic sulfide deposits of Western Australia, *Aust. J. Earth Sci.*, *45*, 265–284, 1998.

Li, C., S.-J. Barnes, E. Makovicky, J. Rose-Hansen, and M. Makovicky, Partitioning on nickel, copper, iridium, platinum, and palladium between monosulfide solid solution and sulfide liquid: Effects of composition and temperature, *Geochim. Cosmochim. Acta*, *60*, 1231–1238, 1996.

Ludwig, K., Isoplot/Ex version 2.3: A Geochronological Toolkit for Microsoft Excel, Spec. Publ. 1a, Berkeley Geochronology Cent., Berkeley, Calif., 2000.

O'Reilly, S. Y., W. L. Griffin, Y. Poudjom Djomani, and P. Morgan, Are lithospheres forever? Tracking changes in subcontinental lithspheric mantle through time, *GSA Today*, *11*, 4–9, 2001.

Pearson, D. G., The age of continental roots, *Lithos*, *48*, 171–194, 1999.

Pearson, D. G., R. W. Carlson, S. B. Shirey, F. R. Boyd, and P. H. Nixon, Stabilization of Archean lithospheric mantle: A Re-Os isotope study of peridotite xenoliths from the Kaapvaal craton, *Earth Planet. Sci. Lett.*, *134*, 341–357, 1995a.

Pearson, D. G., S. B. Shirly, R. W. Carlson, F. R. Boyd, N. P. Pokhilenko, and N. Shimizu, Re-Os, Sm-Nd, and Rb-Sr isotope evidence for the thick Archaean lithospheric mantle beneath the Siberian craton modified by multistage metasomatism, *Geochim. Chosmochim. Acta*, *59*, 959–977, 1995b.

Pearson, D. G., G. A. Snyder, S. B. Shirey, L. A. Taylor, R. W. Carlson, and N. V. Sobolev, Archaean Re-Os age for Siberian eclogites and constraints on Archean tectonics, *Nature*, *374*, 711–713, 1995c.

Pearson, D. G., S. B. Shirey, G. P. Bulanova, R. W. Carlson,

and H. J. Milledge, Re-Os isotopic measurements of single sulfide inclusions in a Siberian diamond and its nitrogen aggregation systematics, *Geochim. Cosmochim. Acta*, *63*, 703–711, 1999.

Pearson, N. J., O. Alard, W. L. Griffin, S. E. Jackson, and S. Y. O'Reilly, In situ measurement of Re-Os isotopes in mantle sulfides by laser ablation multi-collector inductively-coupled mass spectrometry: Analytical methods and preliminary results, *Geochim. Cosmochim. Acta*, *66*, 1037–1050, 2002.

Pokhilenko, N. P., N. V. Sobolev, S. S. Kuligin, and N. Shimizu, Peculiarities of distribution of pyroxenite paragenesis garnets in Yakutian kimberlites and some aspects of the evolution of the Siberian craton lithospheric mantle, *Proc. 7th Int. Kimb. Conf.*, edited by J. J. Gurney et al., pp. 689–698, Red Roof Design, Cape Town, 1999.

Richardson, S. H., S. B. Shirey, J. W. Harris, and R. W. Carlson, Archean subduction recorded by Re-Os isotopes in eclogitic sulfide inclusions in Kimberley diamonds, *Earth Planet. Sci. Lett.*, *191*, 257–266, 2001.

Rosen, O. M., K. C. Condie, L. M. Natapov, and A. D. Nozhkin, Archean and early Proterozoic evolution of the Siberian Craton: a preliminary assessment, in *Archean Crustal Evolution*, edited by K. Condie, pp. 411–459, Elsevier Sci., New York, 1994.

Schoenberg, R., T. F. Nagler, and J. K. Kramers, Precise Os isotope ratio and Re-Os isotope dilution measurements down to the picogram level using multicollector inductively coupled plasma mass spectrometry, *Int. J. Mass Spectrom.*, *197*, 85–94, 2000.

Shirey, S. B., Re-Os compositions of midcontginent rift system picrites: Implications for plume-lithosphere interaction and enriched mantle sources, *Can. J. Earth Sci.*, *34*, 489–503, 1997.

Shirey, S. B., and R. J. Walker, The Re-Os isotope system in cosmochemistry and high-temperature geochemistry, *Annu. Rev. Earth Planet. Sci.*, *26*, 423–500, 1998.

Shirey, S. B., R. W. Carlson, S. H. Richardson, A. Menzies, J. J. Gurney, D. G. Pearson, J. W. Harris, and U. Wiechert, Archean emplacement of eclogitic components into the lithospheric mantle during formation of the Kaapvaal Craton, *Geophys. Res. Lett.*, *28*, 2509–2512, 2001.

Van Acterbergh, E., RockMas modal analysis software, internal rep., 15 pp., Geochem. Evol. and Metal. of Continents (GEOMC), Sydney Aust., 2000.

Volkening, J., T. Walczyk, and K. G. Heumann, Osmium isotope ratio determinations by negative thermal ionization mass spectrometry, *Int. J. Mass Spectrom. Ion Processes*, *151*, 147–159, 1991.